



TECHNICAL UNIVERSITY OF CRETE  
SCHOOL OF CHEMICAL AND ENVIRONMENTAL ENGINEERING  
POSTGRADUATE STUDIES PROGRAMME – ENVIRONMENTAL ENGINEERING

Postgraduate Dissertation Study

**“Optimization of the Canadian Fire Weather Index (FWI) for the  
Mediterranean region”**

**Name: Panagiotis Angelis**

**RN: 2020057527**

Supervising Professor: Apostolos Voulgarakis

Examination Committee:

Apostolos Voulgarakis

Emmanouil Grillakis

Aristeidis Koutroulis

Chania, 2023

## Acknowledgements

Firstly, I would like to thank my Supervising Professor Apostolos Voulgarakis, for giving me the opportunity to work on such an interesting and important research field. His excellent guidance and cooperation greatly enriched my experience throughout the duration of my dissertation study.

Moreover, I would like to thank Dr. Emmanouil Grillakis and PhD Candidate Rovithakis Anastasios, who generously shared their time and knowledge on multiple occasions throughout the duration of my dissertation study.

Additionally, I would like to thank Associate Professor Aristeidis Koutroulis for his valuable contribution as a member of the examination committee.

Finally, I would like to thank my family and friends for supporting me on this journey.

## Abstract

Fire weather prognosis tools are of great importance for mitigating the catastrophic impacts of wildfires posed on human lives, valuable resources and assets. Their importance is getting higher if we reflect on the side effects of climate change such as rising temperatures, extreme drought phenomena and shifting precipitation patterns. These factors contribute to the heightened frequency and severity of wildfires. The Canadian Fire Weather Index (FWI) System stands out as one of the most extensively used tools for fire weather prognosis. Its reliability has been demonstrated across various forest types worldwide. Nevertheless, the FWI equations were initially developed within Canadian boreal forests, which possess different characteristics compared to other forest types, like Mediterranean forests, in terms of their vegetation and climatic conditions. The goal of this project is to refine the already effective Canadian Fire Danger System (FWI) and tailor it for the different characteristics of the Mediterranean climate reference region in order to get improved fire weather prognosis for that particular geographical region.

The first part of the study is finding constants in the equations of the FWI that result from empirical calculations or laboratory tests with region specific characteristics and altering them so as to get different FWI values, that give better or worse fire weather prognosis. Each alteration is rated as better or worse depending on its correlation yield between the corresponding FWI values and Burned Area. The second part of the study is correlating the variables mentioned above using two methods. The first method is the correlation of all the grid boxes of the study region with Burned Area data and the second is the correlation on each grid box by itself providing that enough data of Burned Area is available for it.

Firstly, this study indicates that an underlying positive correlation exists between the average monthly FWI values and the logBA values, which confirms the reliability of the Canadian FWI System. Secondly, using the first method of correlation, the altered FWI codes showed an increase in correlation of up to 10%, suggesting that optimizing the FWI for the Mediterranean climate reference region is feasible. However, it is noticed that despite accomplishing the goal of increased correlation, there is a noticeable difference between the FWI values of the optimized and original FWI code. Special attention should be given on this observation, since certain FWI values are associated with certain fire risk thresholds for different regions. Moreover, using the second method of correlation, from the Figures of Correlation Map and Correlation Map Difference, no clear pattern of increase or decrease in correlation was observed, throughout the study region. This pattern could be cleared out, either by using a broader study period or by accounting for the land use and vegetation type of each gridbox.

# Table of Contents

Acknowledgements .....	2
Abstract.....	3
1. Introduction .....	7
1.1. Motivation.....	7
1.2. Methods Overview.....	7
2. Literature Review .....	8
2.1. Mediterranean Region & Climate .....	8
2.2. Climate Reference Regions .....	11
2.3. Fire regime in the Mediterranean Region.....	12
2.4. Forest Fire Danger Rating Systems and Indices .....	13
2.5. Canadian Forest Fire Weather Index .....	15
2.6. Calibrations/Modifications of FWI.....	17
3. Data.....	18
3.1. Data Gathering.....	18
3.2. Data Preparation.....	19
4. Methodology.....	20
4.1. FWI Calculation .....	20
4.2. Correlation .....	20
4.3. Correlation Map.....	20
4.4. FWI Optimization .....	21
4.5. Study Region .....	27
5. Results.....	28
5.1. Original FWI code.....	28
5.2. Experiment 1 – FFMC (Ed).....	33
5.3. Experiment 2 – FFMC (Ew).....	35
5.4. Experiment 3 – ISI .....	37
5.5. Experiment 4 – DMC .....	39
5.6. Combinations .....	41
5.6.1. Combination 1-2-3 .....	41
5.6.2. Combination 1-2-3-4.....	43

5.6.3. Combination 3-4.....	45
6. Discussion.....	47
7. Conclusions .....	47
8. References .....	48

## Table of Figures

Figure 1. Location of the five Mediterranean climate regions in the world (Bonada and Resh, 2013). .....	8
Figure 2. Landscape diversity within the Mediterranean climate region of the Mediterranean Basin (Bonada and Resh, 2013). .....	9
Figure 3. Köppen-Geiger climate type map of the World (Peel et al., 2007). .....	10
Figure 4. Updated IPCC reference land (grey shading) and ocean (blue shading) regions; note that the Caribbean (CAR), Southeast Asia (SEA) and the Mediterranean (MED) are considered both land and ocean regions (defined using the land and sea masks, respectively). Land masks are used to obtain land-only information for land regions (excluding the coastal white regions) (Iturbine et al., 2020).....	11
Figure 5. Updated Australian Fire Danger Rating ( <a href="https://afdrs.com.au">https://afdrs.com.au</a> ). .....	14
Figure 6. Structure of the FWI System and their connection ( <a href="https://www.nwccg.gov">https://www.nwccg.gov</a> ). .....	16
Figure 7. Isotherm curves of Equilibrium moisture content versus relative humidity at 21.1°C (Van Wagner, 1987). .....	22
Figure 8. Effect of wind speed on relative spread rate in the ISI, along with wind effects from five sources (Shape and slope of curves is relevant, their relative position is not) (Van Wagner, 1987). .....	24
Figure 9. Effect of fine fuel moisture (FFM) on relative spread rate in the ISI, along with FFM effects from three sources (Shape and slope of curves is relevant, their relative position is not) (Van Wagner, 1987). .....	25
Figure 10. Mediterranean Climate Reference Region (LON: 10° W to 40° E, LAT: 30° N to 45° N) (Iturbine et al., 2020). .....	27
Figure 11. Vegetation land cover across the Mediterranean Climate Reference Region & Land Cover Classification ( <a href="https://land.copernicus.eu/global/products/lc">https://land.copernicus.eu/global/products/lc</a> ). .....	27
Figure 12. Fluctuation of the Average FWI values across the Mediterranean Climate Reference Region. ....	28
Figure 13. Correlation of the monthly logBA values and the average monthly FWI values.....	29
Figure 14. Correlation of the monthly logBA values and the average monthly FWI values (bins of 100). .....	30
Figure 15. Correlation of the monthly logBA values and the average monthly FWI values (bins of 100) (logBA>1.7). .....	31
Figure 16. Correlation of the monthly logBA values and the average monthly FWI values on the grid box level (logBA>1.7) (months of BA≥5). .....	32
Figure 17. Correlation of the monthly logBA values and the average monthly FWI values on the grid box level (logBA>1.7) (months of BA≥5) (JJAS). .....	32

Figure 18. Experiment 1 – Pearson’s r for all the sets of multip & expon.....	33
Figure 19. Difference in Pearson’s r between the best fit of Experiment 1 and the original code on the grid box level (logBA>1.7) (months of BA≥5).....	34
Figure 20. Difference in Pearson’s r between the best fit of Experiment 1 and the original code on the grid box level (logBA>1.7) (months of BA≥5) (JJAS).....	34
Figure 21. Experiment 2 – Pearson’s r for all the sets of multip & expon.....	35
Figure 22. Difference in Pearson’s r between the best fit of Experiment 2 and the original code on the grid box level (logBA>1.7) (months of BA≥5).....	36
Figure 23. Difference in Pearson’s r between the best fit of Experiment 2 and the original code on the grid box level (logBA>1.7) (months of BA≥5) (JJAS).....	36
Figure 24. Experiment 3 – Pearson’s r for all the sets of expon1 & expon2. ....	37
Figure 25. Difference in Pearson’s r between the best fit of Experiment 3 and the original code on the grid box level (logBA>1.7) (months of BA≥5).....	38
Figure 26. Difference in Pearson’s r between the best fit of Experiment 3 and the original code on the grid box level (logBA>1.7) (months of BA≥5) (JJAS).....	38
Figure 27. Experiment 4 – Pearson’s r for all the sets of var1 & var2. ....	39
Figure 28. Difference in Pearson’s r between the best fit of Experiment 4 and the original code on the grid box level (logBA>1.7) (months of BA≥5).....	40
Figure 29. Difference in Pearson’s r between the best fit of Experiment 4 and the original code on the grid box level (logBA>1.7) (months of BA≥5) (JJAS).....	40
Figure 30. Correlation of the monthly logBA values and the average monthly FWI values (bins of 100) (logBA>1.7) (Combination 1-2-3).....	41
Figure 31. Difference in Pearson’s r between Combination 1-2-3 and the original code on the grid box level (logBA>1.7) (months of BA≥5). ....	42
Figure 32. Difference in Pearson’s r between Combination 1-2-3 and the original code on the grid box level (logBA>1.7) (months of BA≥5) (JJAS). ....	42
Figure 33. Correlation of the monthly logBA values and the average monthly FWI values (bins of 100) (logBA>1.7), (Combination 1-2-3-4).....	43
Figure 34. Difference in Pearson’s r between Combination 1-2-3-4 and the original code on the grid box level (logBA>1.7) (months of BA≥5). ....	44
Figure 35. Difference in Pearson’s r between Combination 1-2-3-4 and the original code on the grid box level (logBA>1.7) (months of BA≥5) (JJAS). ....	44
Figure 36. Correlation of the monthly logBA values and the average monthly FWI values (bins of 100) (logBA>1.7), (Combination 3-4). ....	45
Figure 37. Difference in Pearson’s r between Combination 3-4 and the original code on the grid box level (logBA>1.7) (months of BA≥5).....	46
Figure 38. Difference in Pearson’s r between Combination 3-4 and the original code on the grid box level (logBA>1.7) (months of BA≥5) (JJAS).....	46

# 1. Introduction

## 1.1. Motivation

Climate change is expected to affect almost every environmental and societal aspect. Some of its side effects are increasing temperatures, drought phenomena and shifting precipitation patterns. These side effects are directly affecting the frequency and intensity of wildfires, creating new fire-prone regions and more severe fire weather behavior (Grillakis 2019, Júnior et al., 2022). Recent studies for southern Europe project an increase in future fire danger and burnt areas varying, on average, from 2 to 4% and from 5 to 50% per decade, respectively (Dupuy et al., 2020).

Wildfires not only threaten the forests and ecosystems, but also pose a great threat to human lives and available resources and assets. (Peris-Llopis et al., 2020). Thus, being able to predict the danger of wildfire events is of great importance for reducing its catastrophic effects. Fire Danger Rating Systems are a great tool for fire prognosis used around the world (Junior et al., 2022). Additionally, as fire and land management agencies are dealing with increased number of fires having limited financial resources, the reliability of fire danger predictive models is becoming a crucial and ever-growing concern in the Mediterranean region (Chelli et al., 2015).

The Canadian Fire Weather Index (FWI) System is one of the most widely used systems for fire weather prognosis, due to its robust results in different types of forests around the world. However, the FWI equations were originally processed and tested in Canadian boreal forests, which have different characteristics from other types of forests such as Mediterranean forests, regarding its vegetation and climate (Chelli et al., 2015).

Thus, by keeping the already successful Canadian Fire Danger System (FWI) and optimizing it for a specific type of forest such as the Mediterranean forest, will result in even better fire prognosis for that specific area. The goal of this project is to optimize the FWI Code for the Mediterranean climate reference region, in order to get better fire prognosis for the specific area.

## 1.2. Methods Overview

The method for this project is firstly, to find constants in the equations of the FWI that are calculated either empirically or in the laboratory with region specific characteristics. Secondly, to alter them in both directions (higher and lower values than the original ones). Finally, ending up with an altered FWI code that gives either better or worse fire prognosis for the study area.

In this project, the rating of “better” or “worse” fire prognosis is done by correlating the following two variables, a) average monthly FWI values and b) monthly logBA (logarithm of Burned Area) values. By changing parameters of the FWI code, the average monthly FWI values change and so does the correlation with the monthly logBA. The optimization of the FWI code is accomplished, on the occasions that the correlation gets stronger. This correlation is studied in two methods, a) on all the grid boxes of the study region with Burned Area data, and b) on each grid box by itself providing that enough data of Burned Area is available for it.

## 2. Literature Review

### 2.1. Mediterranean Region & Climate

The Mediterranean geographic region, is regarded as the area that encloses the Mediterranean Basin and it consists of three continents: southern Europe, southwestern Asia, and northern Africa. Today, 21 countries have coastlines on the Mediterranean Basin. These include Albania, Algeria, Bosnia and Herzegovina, Croatia, Cyprus, Egypt, France, Greece, Israel, Italy, Lebanon, Libya, Malta, Monaco, Montenegro, Morocco, Slovenia, Spain, Syria, Tunisia, and Turkey (<https://www.medqsr.org>).

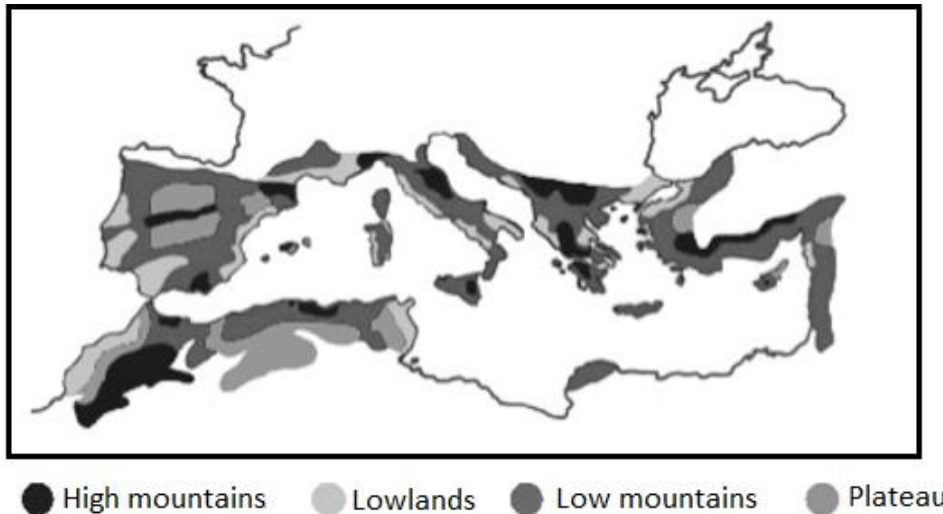
It should be pointed out that the term “Mediterranean” not only refers to a geographical region but also to a climatic zone. The Mediterranean climate is part of the qualitative classification system for the various climate types found on Earth, as established by “Köppen in 1936” and it has also been applied to describe the climate of other regions, typically smaller than the Mediterranean itself. The Mediterranean climate is typically characterized by relatively mild and wet winters, and hot and dry summers and it may be found on the western side of continents in the latitudes between approximately 30 and 45 degrees. The five distinct geographic regions characterized by the Mediterranean climate are i) Mediterranean Basin, ii) Coastal California, iii) Central Chile, iv) the Cape region of Southwestern Africa, and v) the Southwestern and Southern parts of Australia (Figure 1) (Lionello et al., 2006, Bonada and Resh, 2013).



Figure 1. Location of the five Mediterranean climate regions in the world (Bonada and Resh, 2013).

The Mediterranean region includes most of the Atlantic coast of Morocco and Portugal but excludes the biggest parts of Libya and Egypt due to their aridity. It spans over an area of about 1,100,000 km<sup>2</sup> and is located between 31 and 45 degrees of latitude. The landscape of the area is diverse (Figure 2).

On the one hand, it features several elevated mountain regions such as the Betic Cordillera located in the Southern and Eastern Iberian Peninsula, the Taurus Mountains located in Southern Turkey, the Atlas Mountains located in Northwestern Africa, the Kabylia Mountains located in North Algeria and the Mediterranean Alps (which is part of the Alps as an interzonal mountain system) stretching across France, Monaco, Italy and Slovenia. On the other hand, it features lower hills and plains that are common along the coast. In addition, elevated plains can be found in some inland regions. The primary vegetation in the area consists of evergreen trees and shrubs (commonly called “maquia” or “garrigue”), savannas, even dry steppe in the driest parts of the region. There are also numerous deciduous species in the wetter and more mountainous areas (Grove & Rackham, 2001) (<https://www.pbs.org>).



*Figure 2. Landscape diversity within the Mediterranean climate region of the Mediterranean Basin (Bonada and Resh, 2013).*

More specifically, according to Köppen's method of climate classification, the Mediterranean climate is classified as “warm temperate climate with dry summer” or the “Cs” type, which is divided into two subtypes, the “Csa” type (“a” standing for hot summer) and the “Csb” type (“b” standing for warm summer) (Khlebnikova, 2009, Kottek et al., 2006). On Figure 3, an updated version of Köppen-Geiger climate type map of the World is viewed.

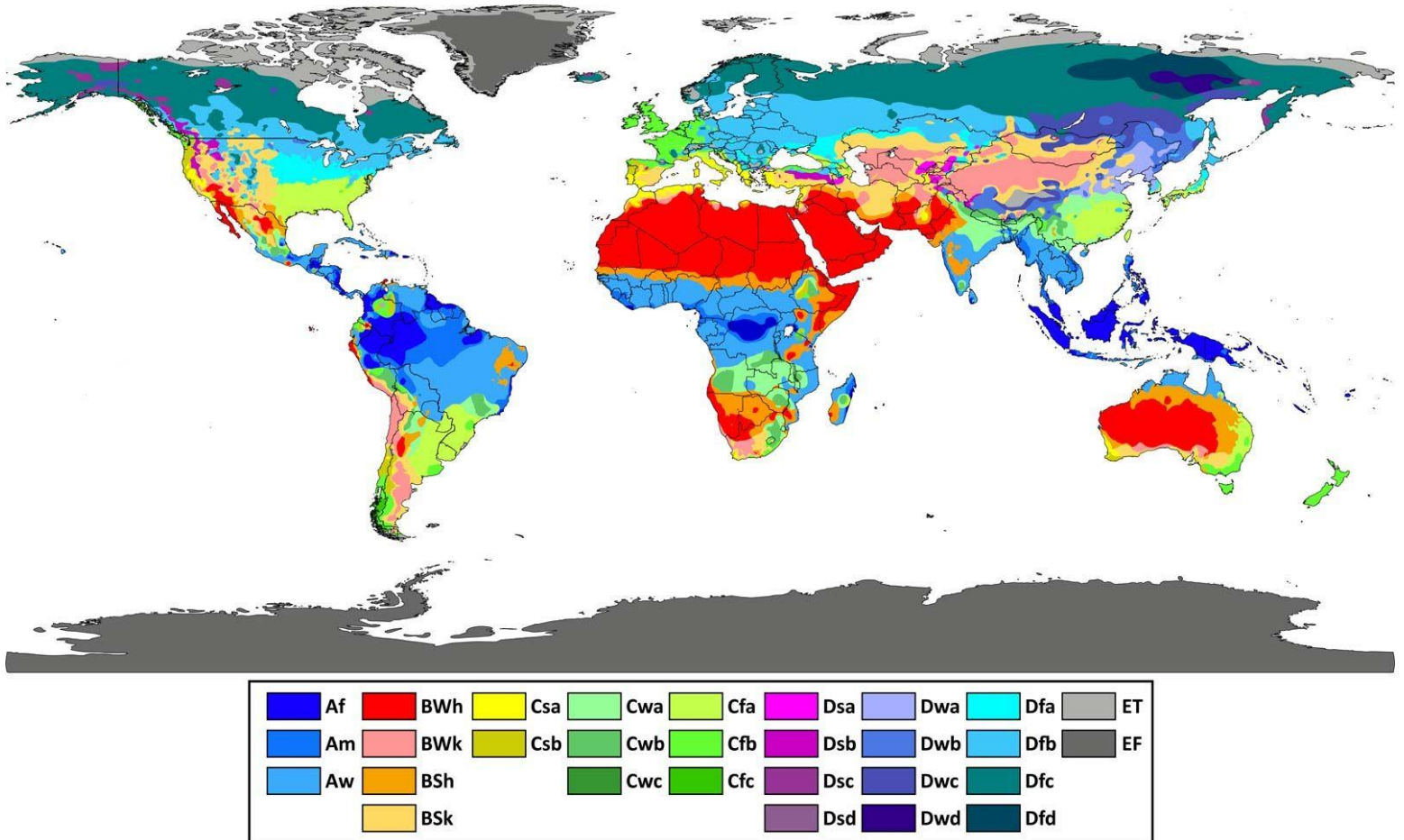


Figure 3. Köppen-Geiger climate type map of the World (Peel et al., 2007).

## 2.2. Climate Reference Regions

Several classifications of climate reference regions have been suggested in the scientific literature for synthesizing historical climate data and projecting future climate change trends in specific geographic areas. These classifications have been employed in multiple assessment reports of the IPCC. The climate reference regions divide the different geographic areas into rectangular shapes with the goal of having climatic consistency and coherency for each shape. These sets of regions, also referred as IPCC WGI reference regions (v4), have been revised many times, so as to represent regional climate features and model results with higher reliability, by also keeping an adequate number of grid boxes per region (Iturbine et al., 2020). Climatic homogeneity is determined by evaluating the average temperature and precipitation using Köppen–Geiger climatic regions (Rubel and Kottke, 2010), taking into consideration the annual cycle and projected changes over the reference regions.

The 4<sup>th</sup> and latest version conclude with 46 land and 15 ocean regions (Figure 4). More specifically, the Mediterranean climate reference region is delimited between 10° W to 40° E longitude and 30° N to 45° N latitude (<https://github.com/SantanderMetGroup/ATLAS>).

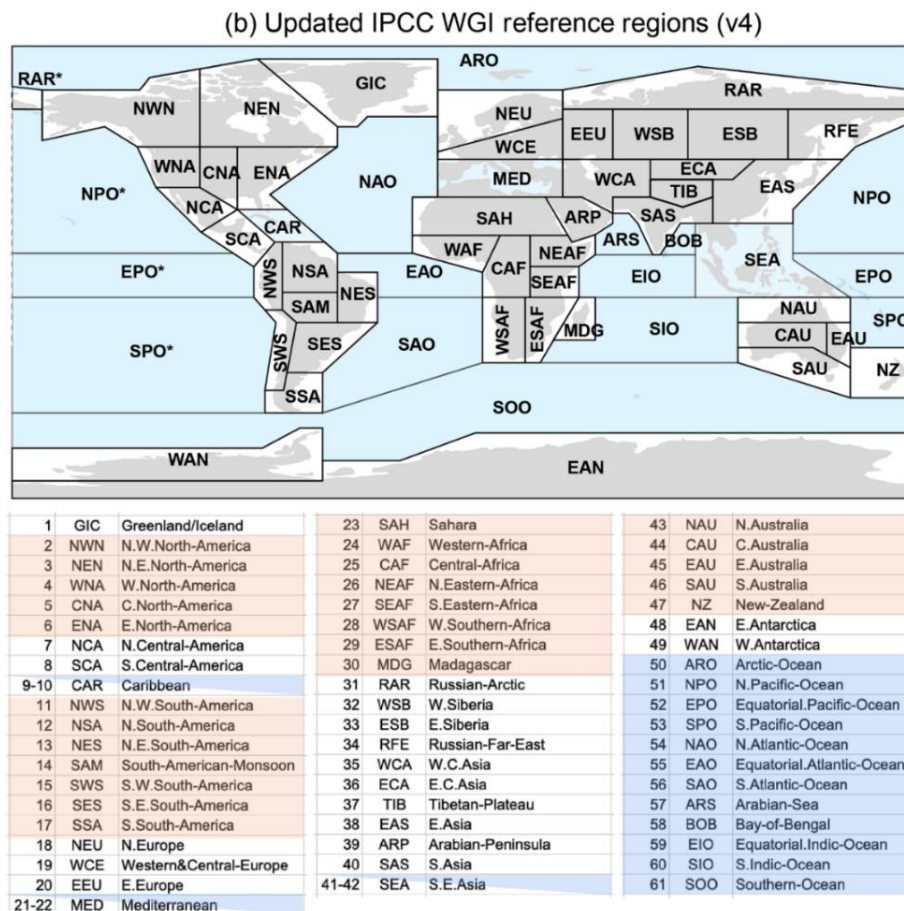


Figure 4. Updated IPCC reference land (grey shading) and ocean (blue shading) regions; note that the Caribbean (CAR), Southeast Asia (SEA) and the Mediterranean (MED) are considered both land and ocean regions (defined using the land and sea masks, respectively). Land masks are used to obtain land-only information for land regions (excluding the coastal white regions) (Iturbine et al., 2020).

### 2.3. Fire regime in the Mediterranean Region

Wildfires are a natural phenomenon in many ecosystems worldwide, and research suggests that the fire regime of a certain region, plays a crucial role in shaping the distribution of species and the overall vegetation dynamics of landscapes. The term “fire regime” refers to the combination of wildfire frequency, intensity, seasonality, and spread pattern. One of these ecosystems is that of the Mediterranean climate, which is commonly acknowledged as “fire-prone”, meaning wildfires have been a natural occurrence for such ecosystems for a long time, dating back to at least the late Quaternary period. Plants in these ecosystems have developed special mechanisms to adapt and cope with wildfires (Chergui et al., 2018, Michelaki et al., 2020).

At the macro level (seasonal time scale), the reason for that behavior is the climate itself, having rainy and mild winters succeeded by warm and dry summers, which causes high levels of vegetation stress, making the Mediterranean region more susceptible to fire events. At the micro level (daily time scale), extreme weather conditions and fuel availability in turn are the significant factors for the initiation and spread of wildfires (DaCamara et al., 2014).

Although fire regimes are typically stable, they do have shifts throughout the years and historically they have been linked to fluctuations in atmospheric oxygen concentration, climate oscillations and sudden alternations of herbivorous animal population. In recent years, fire regimes are mostly affected by the indirect effects of human activities, which causes climate change and by the direct effects of human activities, which include land use change and rural depopulation (Chergui et al., 2018).

More specifically, due to climate change, Europe is expected to experience drought events of unprecedented spatial extent and prolonged duration, occurring as frequently as twice per decade in the future, irrespective of mitigation efforts, which in turn are expected to increase the risk of wildfire events, shorten the time between such events and increase the duration of the fire season, causing severe environmental and economic losses year by year (Grillakis et al., 2019, Rovithakis et al., 2019). Furthermore, the desertion of land resulting from rural depopulation, coupled with land use change and reforestation projects leads to increased levels of fuel connectivity (denser vegetation). Thus, the fire regime switched from fuel limited, to drought driven (Chergui et al., 2018).

Numerous factors, both natural and anthropogenic, contribute to the incidence and spread of forest fires and although human activity is the primary cause of wildfires in regions such as the Mediterranean Basin, natural conditions such as fuel properties and moisture content are the ones with a catalytic role in the ignition and spread of wildfires (Dimitrakopoulos et al., 2011 Zacharakis et al., 2023).

To put numbers into perspective, the Mediterranean region accounts for over 85% of burned area in Europe, being one of the world most affected regions in terms of significant wildfire events. These fires burn around half a million hectares of vegetation cover each year, resulting in substantial economic losses and ecological harm (DaCamara et al., 2014).

In certain southern Mediterranean countries, 2017 has been recorded as one of the most destructive wildfire seasons to date. This was marked by a significant increase in burned area, with Portugal experiencing a 535% increase, France 160%, Italy 105%, and Spain 95%, in comparison to the

typical levels observed in the prior decade (San-Miguel-Ayanz et al. 2018). For Greece, 2021 was the year that saw a significant increase in the burnt area. With five wildfires occurring in less than a month, the extent of burnt land was three times larger than the annual average of the previous decade (Giannaros et al., 2022).

#### 2.4. Forest Fire Danger Rating Systems and Indices

Within the scope of climate analysis, “fire danger” as a term, refers to the assessment of the climatic conditions that determine ignition speed, rate of spread, suppression difficulty and severity of a fire. Therefore, it is crucial to estimate the fire danger a few days (or longer) beforehand to enable fire protection agencies to react quickly and provide sufficient human and material resources (Bedia et al., 2018).

Historically, fire danger prediction primarily relied on statistical techniques that utilized the delayed connections between various fire-related measures (such as the number of fires and the total burnt area) and slowly changing climate system components used as predictors, such as sea-surface temperatures or meteorological droughts. These predictions were also based on meteorological observations, on a global to regional scale. Nevertheless, the use of empirical approaches had its limitations as it relied on the short history of observation-based data, leading to inaccuracies and point observations that were not representative of broader region stations as a result of local small-scale variations in meteorological variables resulting in the loss of data. The use of modern climate science and climate models has allowed for the development of numerical climate models such as Global Climate Models (GCMs). These models generate predictions based on simulations of atmospheric and oceanic parameters, providing an alternative to empirical approaches (Bedia et al., 2018, Ntinopoulos et al., 2022).

However, the predictions from model simulations unavoidably come with a degree of uncertainty due to model biases, resulting in significant deviations from observed climate. To address this, the mean outputs of multiple models, known as ensembles, are often used. Ensembles can provide more confidence in the decision-making process during emergency situations, as a cost-loss analysis can be associated with different scenarios. Running ensembles is computationally intensive, and therefore, they are typically run at lower resolutions than a single deterministic run. The forecast is then interpreted as probabilistic, rather than deterministic (Bedia et al., 2018, Ntinopoulos et al., 2022).

Accordingly, modern fire danger assessment uses the climate predictions from GCMs in combination with Fire Danger Rating Systems and Indices to predict future fire danger with higher certainty. These Fire Danger Rating Systems and Indices are produced through research both in theoretical and in empirical terms and they mostly use meteorological parameters such as temperature, humidity, wind and precipitation in correlation with fuel moisture as well as other parameters, to give off an index that translates into the danger of a fire occurring, or its severity if it were to happen (Zacharakis et al., 2023).

The ability to predict fire danger can reduce the ecological and economic losses as well as operation costs for fire suppression systems. Fire and land management agencies utilize fire danger rating systems

to assess their readiness levels, release public alerts, and establish management, research, and legal frameworks concerning fire-related issues (Dimitrakopoulos et al., 2011).

Different regions of the world implement different fire danger rating systems, including some of the following:

- Fire Weather Index – Canada (FWI, Van Wagner 1987)
- McArthur Forest Fire Danger Index – Eastern parts of Australia (FFDI, McArthur 1967)
- Forest Fire Behaviour Tables – Western Australia (FFBT, Sneeuwjagt and Peet 1998)
- National Fire Danger Rating System – USA (Deeming et al. 1977)

All these systems integrate weather conditions, fuel moisture and other parameters to assess fire danger, calculated as a numerical index. Although fire danger is not the same as fire behavior, the indices were developed on the assumption that fire danger is related to fire behavior, quantified as rate of spread or intensity. Index values are classified into rating classes to aid interpretation. Most systems use five rating classes: Low, Moderate, High, Very High, and Extreme (Matthews, 2009). On Figure 5, an example of Fire Danger rating can be seen.

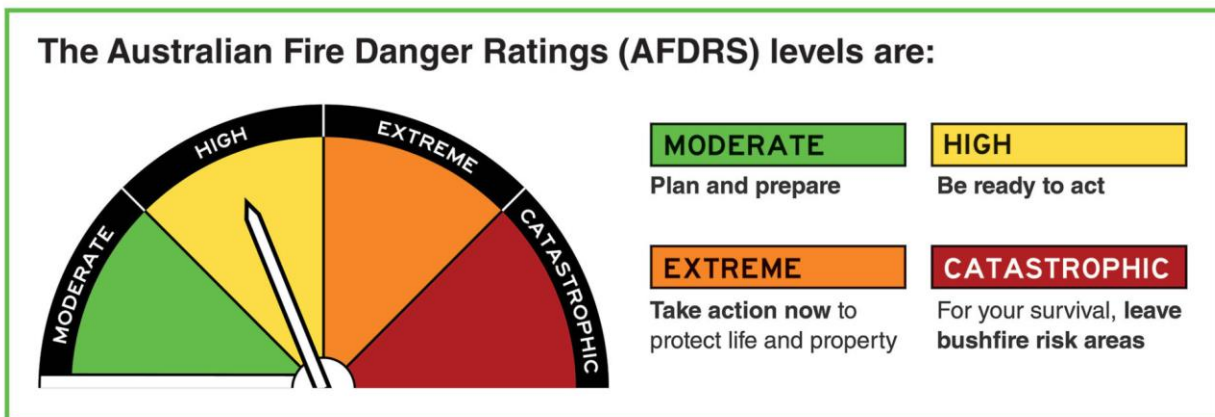


Figure 5. Updated Australian Fire Danger Rating (<https://afdrs.com.au>).

## 2.5. Canadian Forest Fire Weather Index

Among the various fire danger systems being used in literature and in practice, both on global and regional scale, the most frequently used one is the Canadian Forest Fire Weather Index (CFFWI) or Fire Weather Index (FWI) in short, due to its simplicity and robustness (Ntinopoulos et al., 2022, Grillakis et al., 2022). The FWI was developed after years of work by a number of fire researchers in the Canadian Forestry Service (Van Wagner 1987). Data of weather, fuel moisture and test fire behavior were collected and tested over several decades for the final form of the FWI to be produced (Simard and Main, 1982).

The Fire Weather Index (FWI) System is composed of six (6) standard components. The first three are fuel moisture codes that follow daily changes in the moisture content of three classes of forest fuel with different drying rates. The last three (including the FWI itself) are fire behavior indices representing rate of spread, fuel weight consumed and fire intensity (Dimitrakopoulos et al., 2011, Van Wagner 1987).

### 1) FFMC – Fine Fuel Moisture Code

It represents the moisture content of litter and other cured fine fuels in a forest stand, in a layer of dry weight about 0,25 kg/m<sup>2</sup>. This code is an indicator of the relative ease of ignition and flammability of fine fuel.

### 2) DMC – Duff Moisture Code

It represents the moisture content of loosely compacted, decomposing organic matter weighing about 5 kg/m<sup>2</sup> when dry (found around 7 cm of soil depth). Also used as an indicator of the receptivity of the forest floor to ignition by lightning.

### 3) DC – Drought Code

It represents a deep layer of compact organic matter weighing around 25 kg/m<sup>2</sup> when dry. This code is a good indicator on the seasonal drought effect on soil moisture.

### 4) ISI – Initial Spread Index

A combination of wind and the FFMC, and represents the rate of spread alone without the influence of variable quantities of fuel.

### 5) BUI- Buildup Index

A combination of the DMC and the DC, and represents the total fuel available to the spreading of fire.

### 6) FWI – Fire Weather Index

A combination of the ISI and the BUI, and represents the intensity of the spreading fire as energy output rate per unit length of fire front.

The system uses as inputs only weather readings/observations taken each day at noon local standard time (LST), generally specified as 12:00 hours, and those are dry-bulb temperature, air relative humidity, 10m open wind speed and 24 h accumulated precipitation (if any) (Turner and Lawson, 1978).

The structure of the Canadian FWI System and the connections between fire weather observations, fuel moisture codes and fire behavior indices can be viewed on Figure 6.

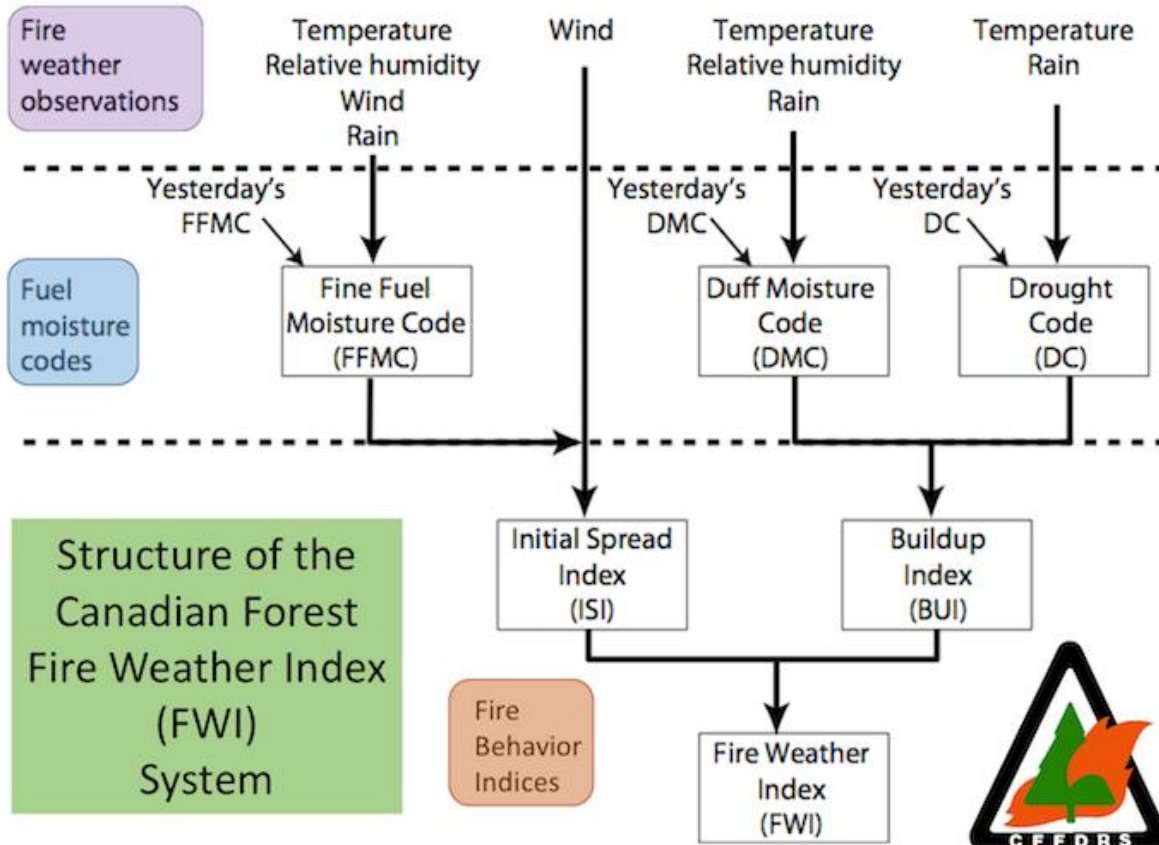


Figure 6. Structure of the FWI System and their connection (<https://www.nwccg.gov>).

In its basic form, the FWI system is a set of equations that can easily be processed by computer, which is a big advantage over the previous systems (Van Wagner and Pickett, 1985).

The FWI system was designed for Canadian fuel and weather conditions and primarily refers to a standard pine fuel type which is pretty common in Canadian forests (Van Wagner 1987). More specifically, the exact fuel type (trees) that were used for the development of the FWI system and more specifically the Equilibrium Moisture Content (EMC) of fine fuel are leaf litter of the following (Van Wagner, 1972):

- White pine (*Pinus Strobus* L.)
- Red pine (*Pinus Resinosa* Ait.)
- Jack pine (*Pinus Banksiana* Lamb.)
- Trembling aspen (*Populus Tremuloides* Michx.)
- Sugar Maple (*Acer saccharum* Marsh.)
- Grass (*Calamagrostis* p.)
- Processed match splints (standard fine fuel in Canadian research on fire danger rating)

## 2.6. Calibrations/Modifications of FWI

The FWI system was originally created to incorporate weather data into indices for fuel moisture and fire danger, with no consideration given to variations in forest types (Wotton, 2009). The FWI equations were developed and tested in boreal forests in Canada, which have different features compared to Mediterranean vegetation and climate. Specifically, the Canadian FWI was designed to monitor moisture in a standard Jack Pine (*Pinus banksiana*) and Lodge Pole Pine (*Pinus contorta*) forest. In contrast to Canadian boreal forests, Mediterranean forests are found in a distinct climate, consisting of different species, and have a simpler vertical structure due to widespread coppice management. Additionally, they are commonly found in marginal areas with shallow soils and low biomass accumulation and have a relatively slow growth rate (Chelli et al., 2015).

There is not much literature in the topic of FWI Optimization/Calibration for different regions and few researchers have attempted this.

Cheli et al. (2015) collected forest fuel moisture data from the regions of Peloponnese and Algarve and calibrated the Fine Fuel Moisture Code (FFMC) and Duff Moisture Code (DMC) to match the collected fuel moisture data in order to improve the FWI code in predicting forest fire danger. This study produced promising results of an adapted FWI code, however, due to the heterogeneity of the Mediterranean vegetation, further testing and research should be made for a more precise calibration of the FWI code.

Yang et al. (2015) focused on calibrating (reformulating) the Drought Code (DC) component of the FWI code for New Zealand. Two methods were investigated. The first method (PotE) replaces the evapotranspiration values, calculated by the FWI code, with values taken from JULES (Joint UK Land Environment Simulator). The second method (soilM) replaces the moisture content of the compact organic matter of the deep layer (referred to as "soil moisture" in this study) calculated by the FWI code, with either observed soil moisture or simulated soil moisture taken from JULES. The results from this study suggest that the original DC method underestimated the drought status, resulting in underestimation of FWI values whereas the PotE method overestimated it. Moreover, the soilM method that used simulated moisture, reduced the errors in the calculated drought status and FWI. Unfortunately, FWI values between the original and the calibrated code were not compared, since there were no records of wildfire around the study area.

## 3. Data

### 3.1. Data Gathering

#### 1. Burned Area (BA)

The satellite data for Burned Area were collected from NASA's Moderate Resolution Imaging Spectroradiometer (MODIS), Global Land Cover Product (MCD64A1) and specifically for the years 2001-2016 on a monthly time resolution. The current dataset has a spatial resolution of  $0.25^\circ$  and provides values of burned area in hectares and information on percentages of burned area for 17 different land types, such as evergreen needleleaf forest, open shrublands or even savannas (Giglio et al., 2018).

#### 2. Climate Data

Meteorological data were collected from the ERA5 dataset, which is the fifth generation of reanalysis for the global climate and weather for the past 8 decades. It is generated by the Copernicus Climate Change Service, which is part of the Earth's monitoring programme of the European Union and implemented by the European Centre for Medium-Range Weather Forecasts (ECMWF) (<https://climate.copernicus.eu>).

Reanalysis is a process that combines data from computer models and observations from all over the world. The aim is to produce a comprehensive observation-based dataset that is consistent with the laws of physics. This is done through a technique called data assimilation, which is similar to what is used by weather forecast centers. In this technique, a previous forecast is combined with new observations to produce a new and improved estimate of the atmosphere's state, which is then used to update future forecasts. Reanalysis works the same way as weather forecasts, but at a lower resolution, allowing for the creation of a dataset that spans several decades. Unlike weather forecasts, reanalysis does not have to be timely, which means there is more time to collect observations and apply retrospectively. This also allows for the incorporation of improved versions of original observations, which ultimately improves the quality of the reanalysis output (Copernicus Climate Change Service, 2023).

Specifically, five meteorological variables and one parameter that separates land and sea grid boxes, all at a  $0.25^\circ$  resolution were collected for the time period of 2001-2016. Those are (Hersbach et al., 2023):

- **10m u-component of wind** (eastward component of wind at a height of 10 meters above the surface of the Earth)
- **10m v-component of wind** (northward component of wind at a height of 10 meters above the surface of the Earth)
- **2m temperature** (temperature of air at 2 meters above the surface of land, sea or inland waters)
- **total precipitation** (accumulated liquid and frozen water, comprising rain and snow, that falls to the Earth's surface)
- **2m dewpoint temperature** (temperature to which the air, at 2 meters above the surface of the Earth, would have to be cooled for saturation to occur)

- **Land-Sea mask** (proportion of land, as opposed to ocean or inland waters)

### 3.2. Data Preparation

The data were prepared for their use in the Mediterranean Climate Reference Region and the Canadian Fire Weather Index System. Data preparation was done on the MATLAB programming platform.

At first, both burned area data and climate data were cropped into certain dimensions, so as to fit the Mediterranean Climate Reference Region. Having 0.25° resolution, the study region comes up to 201 cells in the Longitude (X axis) and 61 cells in the Latitude (Y axis). Resulting in a study region of 201x61 grid boxes.

After that, hourly climate data were converted into daily climate data. This was achieved by keeping only one value out of the 24-hourly values and that is of 12:00 LST (Local Standard Time), as it is a prerequisite in the FWI system. The only exception is total precipitation, where the 24-hourly values of each day were added for the final daily value.

Then, climate data were converted into the four necessary input data for the FWI and those are temperature, relative humidity, 10m open wind speed and 24 h accumulated precipitation. More specifically, 10m u-component of wind and 10m v-component of wind were combined for the calculation of the 10m open wind speed, and 2m dewpoint temperature and 2m air temperature were combined for the calculation of the relative humidity using the formula for saturated water pressure from Wright (1997).

$$wind = \sqrt{wind_u^2 + wind_v^2}$$

$$maximum\ water\ pressure = 611.21 * e^{\frac{17.502 * temp}{240.97 + temp}}$$

$$actual\ water\ pressure = 611.21 * e^{\frac{17.502 * dpt}{240.97 + dpt}}$$

$$rh = \frac{actual\ water\ pressure}{maximum\ water\ pressure} * 100$$

Finally, the Land-Sea mask was applied on the climate data, in order to exclude grid boxes that represent bodies of water (ocean or inland waters) from the FWI calculations.

## 4. Methodology

### 4.1. FWI Calculation

Following the preparation of climate data, the first step of the methodology requires the input of those data into the Canadian FWI system, meaning its equations. The end result from this step, are the daily values of FWI for all the grid boxes of the study region excluding the areas of ocean or inland waters (using the Land-Sea mask), for the years 2001-2016.

All FWI calculations were done on the MATLAB programming platform and the equations used can be seen on the official Canadian Forestry Technical Report of 1987 by Van Wagner.

### 4.2. Correlation

The daily FWI values were then converted into average monthly FWI values and the monthly burned area values were converted into monthly logBA (logarithm of monthly Burned Area values). The use of logBA has been found to be a useful tool for examining correlation between Burned Area and drought or fire indicators over seasonal and interannual time periods in a linear fashion (Abatzoglou et al., 2018, Grillakis et al., 2022).

The two sets of values were paired and sorted by ascending order of the monthly logBA values and were then correlated and the Pearson's  $r$  was calculated.

Then, the two sets of values were binned, having 100 sets of values in each bin, and the correlation process and Pearson's  $r$  calculation was repeated.

Finally, low values of BA were excluded from the correlation and the correlation process and Pearson's  $r$  calculation were repeated once more.

### 4.3. Correlation Map

Furthermore, a different type of correlation was also considered, by correlating the same two variables (average monthly FWI, monthly logBA) on the grid box level, referred to as Correlation Map from here on. Since many grid boxes had very few or no fire events for the time period of the study (2001-2016), grid boxes that experienced less than five months in total (of the 2001-2016 period) of fire events (Burned Area) were excluded from the correlation.

The Correlation Map was also re-made after keeping only 4 months (June-July-August-September – JJAS) of the year, since they represent the peak of the fire season in the Mediterranean Region.

#### 4.4. FWI Optimization

In order to further optimize the FWI code for the specific study region, certain equations of the FWI code that were either empirical or the result of region-specific parameters, were chosen as fit for this study and were altered.

Four different variations were studied, from here on referred to as Experiments, choosing certain equations each time in each of the following indices:

- Experiment 1 - (FFMC – EMC(Ed))
- Experiment 2 - (FFMC – EMC(Ew))
- Experiment 3 - ISI
- Experiment 4 - DMC

The same methodology was followed for all the experiments, obtaining different values of average monthly FWI values, which were then correlated with the same monthly logBA, ending up with a different Pearson's  $r$  in each experiment. Multiple set of values were tested in each Experiment and the highest Pearson's  $r$  value (best fit) of each Experiment was chosen as a tool for comparing the results of the Experiments with those of the original code.

The same methodology was also followed for the second approach, the Correlation Map, which was plotted using the best fit from each Experiment. For the sake of comparison, the Correlation Map of the original code was subtracted from them, as shown on the following equation, where  $i$  and  $j$  are the coordinates of each grid box.

$$\begin{aligned} & \textit{Correlation Map Difference}(i,j) \\ & = \textit{Correlation Map Experiment}(i,j) - \textit{Correlation Map Original}(i,j) \end{aligned}$$

##### **Experiment 1 - FFMC (Ed)**

The first experiment focused on the Fine Fuel Moisture Code – FFMC component of the FWI code and specifically on the Equilibrium Moisture Content – EMC obtained in the drying phase of the fine fuel (Ed).

Moisture of dead vegetative material (leaves, pine needles etc.) comes to an equilibrium with the atmospheric conditions in certain rates, depending on the type of vegetation. This specific rate which is different in each vegetation type, plays a crucial role in the calculation of the FWI value. For that reason, during the years 1960 to 1968, specific experiments took place in a laboratory in order to calculate the drying/wetting rates for fine fuel to reach equilibrium with the daily atmospheric conditions. Canadian local species of tree litter, mainly pine trees, were used in the experiments since they form the biggest part of the Canadian boreal forests (Van Wagner, 1972).

The equation describing the EMC of the drying phase is the Ed equation of the FWI code and describes the drying isotherm curve of Figure 7:

- $E_d = (0.942) * RH^{0.679} + 11 * e^{\frac{RH-100}{10}} + 0.18 * (21.1 - TEMP) * (1.0 - e^{0.115*RH})$

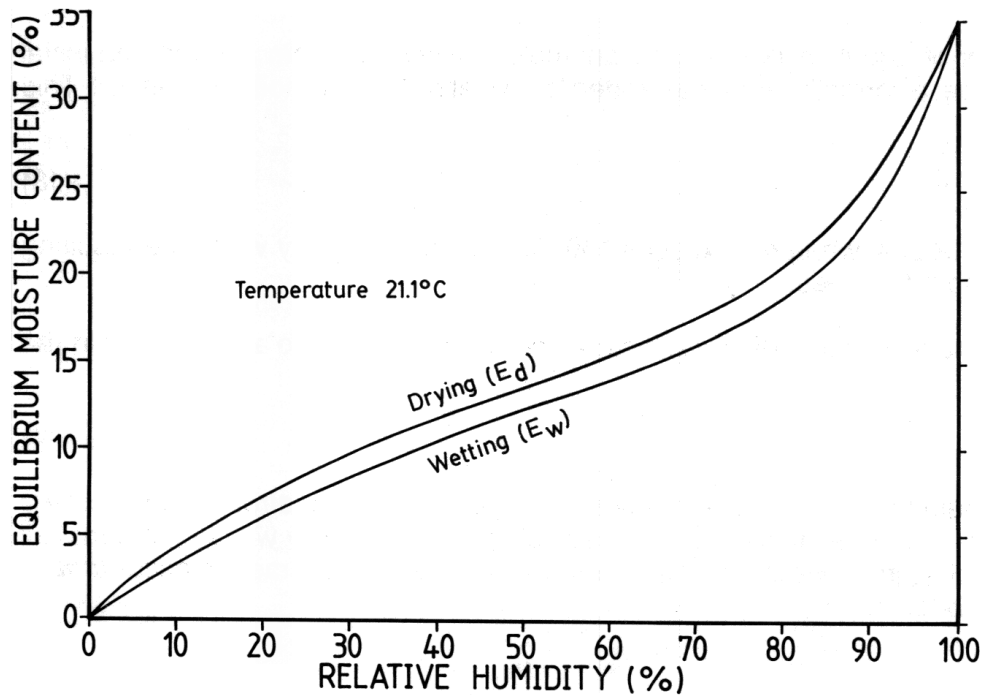


Figure 7. Isotherm curves of Equilibrium moisture content versus relative humidity at 21.1°C (Van Wagner, 1987).

As such, different types of forests (different vegetation), in our case Mediterranean forests, are suggested to be represented by modified Ed equations. In order to do so in a controlled manner, two parameters from the Ed equation were chosen as fit for change. Those are 0.942 and 0.679, which were named *multip* and *expon*, and they are considered variables from here on. The Ed equation, becomes as follows:

- $E_d = (multip) * RH^{expon} + 11 * e^{\frac{RH-100}{10}} + 0.18 * (21.1 - TEMP) * (1.0 - e^{0.115*RH})$

The study utilized different values for the parameters of *multip* and *expon*, represented as percentages of the original parameter values, in order to modify the Ed equation. The percentages ranged from 60% to 120% of the original values as follows:

The values used:

- *multip* = 0.60\*0.942, 0.65\*0.942.....1.15\*0.942, 1.20\*0.942 (total of 13 values)
- *expon* = 0.60\*0.679, 0.65\*0.679.....1.15\*0.679, 1.20\*0.679 (total of 13 values)

A total of 169 sets of values (13 values for each parameter) were used to calculate the average monthly FWI values, which were then correlated with monthly logBA values.

## Experiment 2 - FFMC (Ew)

The second experiment focused on the Fine Fuel Moisture Code – FFMC component of the FWI code and specifically on the Equilibrium Moisture Content – EMC obtained in the wetting phase of the fine fuel (Ew).

The equation describing the EMC of the drying phase is the Ew equation of the FWI code and describes the wetting isotherm curve of Figure 7:

- $$E_w = (0.618) * RH^{0.753} + 10 * e^{\frac{RH-100}{10}} + 0.18 * (21.1 - TEMP) * (1.0 - e^{0.115*RH})$$

Again, two parameters from the Ew equation were chosen as fit for change. Those are 0.618 and 0.753, which were named *multip* and *expon*, and they are considered variables from here on. The Ew equation, becomes as follows:

- $$E_w = (multip) * RH^{expon} + 10 * e^{\frac{RH-100}{10}} + 0.18 * (21.1 - TEMP) * (1.0 - e^{0.115*RH})$$

Using the same method as in the previous experiment, in the place of *multip* and *expon*, different set of values were used ranging from 60% to 120% of the original value.

The values used:

- *multip* = 0.60\*0.618, 0.65\*0.618.....1.15\*0.618, 1.20\*0.618 (total of 13 values)
- *expon* = 0.60\*0.753, 0.65\*0.753.....1.15\*0.753, 1.20\*0.753 (total of 13 values)

A total of 169 sets of values (13 values for each parameter) were used to calculate the average monthly FWI values, which were then correlated with monthly logBA values.

### Experiment 3 - ISI

The third experiment focused on the Initial Spread Index – ISI component of the FWI code and specifically on two equations. The first one represents the wind effect,  $f(W)$ , and the second one represents the fine fuel moisture effect,  $f(F)$ , on the spread rate of fire. Their effect can be viewed on Figure 8 and Figure 9.

The above-mentioned equations were chosen as fit for change, since they are essentially empirical. Specifically for the first equation, its validity is uncertain at very high wind speeds (Van Wagner, 1987).

#### 1<sup>st</sup> Equation

- $f(W) = e^{0.05039*W}$

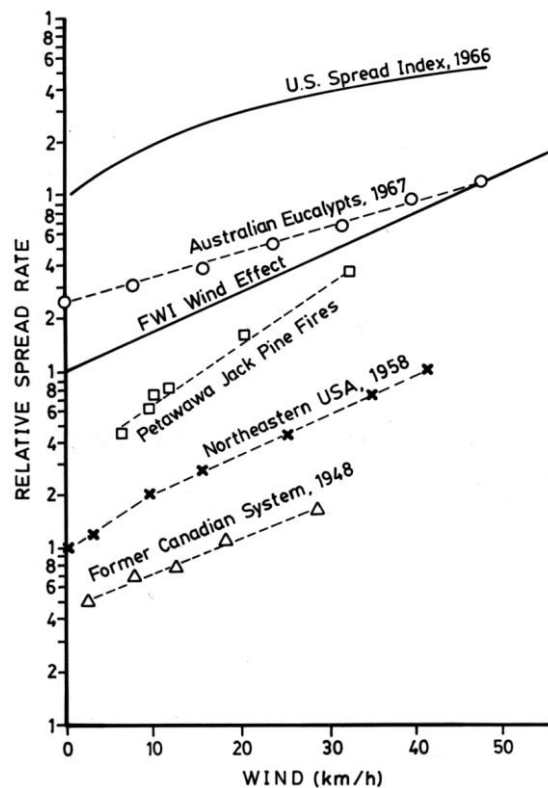


Figure 8. Effect of wind speed on relative spread rate in the ISI, along with wind effects from five sources (Shape and slope of curves is relevant, their relative position is not) (Van Wagner, 1987).

The equation  $f(W)$  has only one parameter, the exponent 0.05039, which was chosen, named  $expon1$  and is considered a variable from here on. The  $f(W)$  equation, becomes as follows:

- $f(W) = e^{expon1*W}$

2<sup>nd</sup> Equation

$$\bullet f(F) = (91,9 * e^{-0.1386*m}) \left[ \frac{1+m^{5.31}}{4.93*10^7} \right]$$

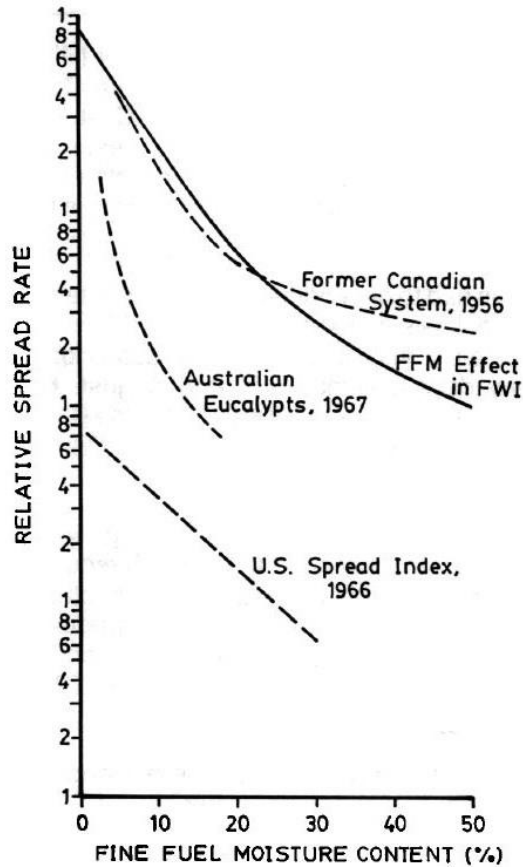


Figure 9. Effect of fine fuel moisture (FFM) on relative spread rate in the ISI, along with FFM effects from three sources (Shape and slope of curves is relevant, their relative position is not) (Van Wagner, 1987).

The equation  $f(F)$  has more than one parameter, however the exponent 0.1386, was chosen, named  $expon2$  and is considered a variable from here on. The  $f(F)$  equation, becomes as follows:

$$\bullet f(F) = (91.9 * e^{-expon2*m}) \left[ \frac{1+m^{5.31}}{4.93*10^7} \right]$$

Using the same method as in the previous experiment, in the place of  $expon1$  and  $expon2$ , different set of values were used ranging from 60% to 120% of the original value.

The values used:

- $expon1 = 0.60*0.05039, 0.65*0.05039, \dots, 1.15*0.05039, 1.20*0.05039$  (total of 13 values)
- $expon2 = 0.60*0.1386, 0.65*0.1386, \dots, 1.15*0.1386, 1.20*0.1386$  (total of 13 values)

A total of 169 sets of values (13 values for each parameter) were used to calculate the average monthly FWI values, which were then correlated with monthly  $\log BA$  values.

#### Experiment 4 – DMC

The fourth experiment focused on the Duff Moisture Code – DMC component of the FWI code and specifically on two equations concerning the wetting phase of the duff layer. The first one represents the calculation of the moisture content of the duff layer according to the previous day's DMC and the second one represents today's DMC according to the previously calculated moisture content.

DMC represents the moisture content of real slow drying forest fuel. The duff layer was chosen as a representative fuel type due to its constant occurrence in Canadian forests. The development of DMC equations was the result of four years of fieldwork, mainly in red pine and jack pine forests (Van Wagner 1987).

For that reason, different types of forests (different vegetation), in our case Mediterranean forests, have different type of duff layer (decomposing organic matter in the same soil depth) and should be represented by modified DMC equations.

The two equations are the following:

- $M_o = 20 + e^{\left(\frac{5.6348 - DMC_{prev}}{43.43}\right)}$
- $P_r = 244.72 - 43.43 * \log(M_r - 20) \rightarrow P_r = 43.43 * (5.6348 - \log(M_r - 20))$

The  $P_r$  equation is slightly re-arranged, in order to end up with the same parameters as the  $M_o$  equation. The above equations have three parameters, two of them were chosen as fit for change. The first is 5.6348, named var1 and the second one is 43.43 named var2 and they are considered variables from here on. The equations, become as follows:

- $M_o = 20 + e^{\left(\frac{var1 - DMC_{prev}}{var2}\right)}$
- $P_r = var2 * (var1 - \log(M_r - 20))$

Using the same method as in the previous experiment, in the place of var1 and var2, different set of values were used ranging from 60% to 120% of the original value.

The values used:

- var1 = 0.60\*5.6348, 0.65\*5.6348.....1.15\*5.6348, 1.20\*5.6348 (total of 13 values)
- var2 = 0.60\*43.43, 0.65\*43.43.....1.15\*43.43, 1.20\*43.43 (total of 13 values)

A total of 169 sets of values (13 values for each parameter) were used to calculate the average monthly FWI values, which were then correlated with monthly logBA values.

#### Combinations

Lastly, combinations of the above-mentioned Experiments were carried out for the FWI calculations. These combinations integrated the alteration/modifications that yielded the highest Pearson's r value in each experiment. By incorporating multiple optimization Experiments, the correlation of the two variables is expected to increase.

#### 4.5. Study Region

The region analyzed in this study is the Mediterranean Climate Reference Region as used in the updated IPCC WGI reference regions (v4) (Iturbine et al., 2020). As mentioned before, the specific region is delimited between 10° W to 40° E longitude and 30° N to 45° N latitude. In Figure 10 the study region is viewed in more detail. Moreover, a map of the vegetation land cover is viewed on Figure 11 and its land cover classification on Figure 12, provide an insight of the study region regarding its vegetation/fire dynamics.

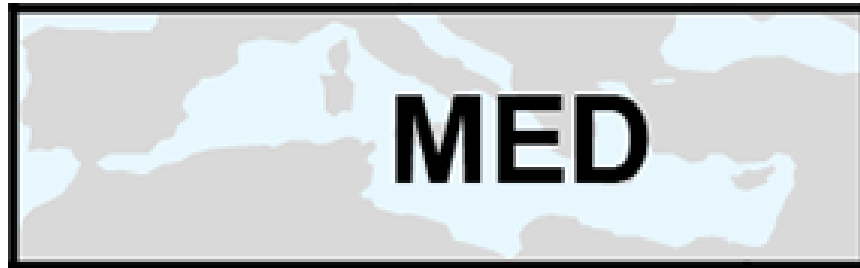


Figure 10. Mediterranean Climate Reference Region (LON: 10° W to 40° E, LAT: 30° N to 45° N) (Iturbine et al., 2020).

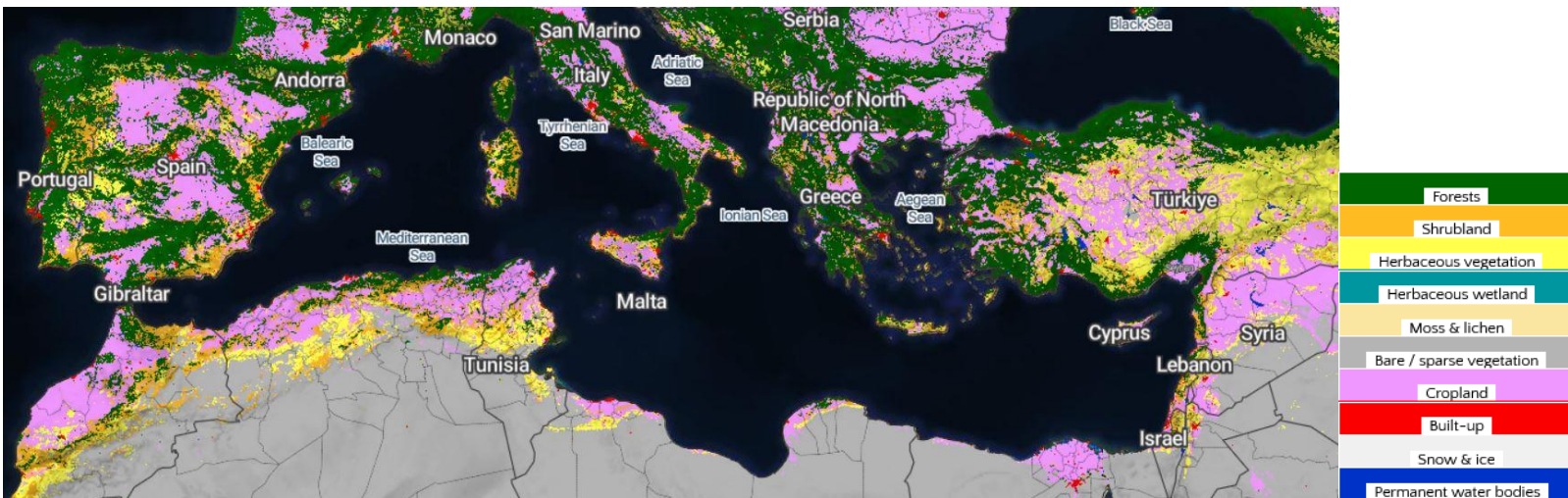


Figure 11. Vegetation land cover across the Mediterranean Climate Reference Region & Land Cover Classification (<https://land.copernicus.eu/global/products/lc>).

A quick observation is that areas located at the Northern parts of Africa and Western parts of Asia, such as parts of Morocco, Algeria, Tunisia, Libya, Egypt and Syria, have more favorable conditions for fire events (higher temperature, lower humidity etc.), however, the high percentages of bare/sparse vegetation make wildfires uncommon in these places.

## 5. Results

### 5.1. Original FWI code

First of all, a map of the average FWI was plotted (Figure 12), for the study region and the study period, in order to have a clear view of the fluctuations of the average FWI values across the Mediterranean climate reference region. The original equations of the Canadian FWI were used (Van Wagner, 1987).

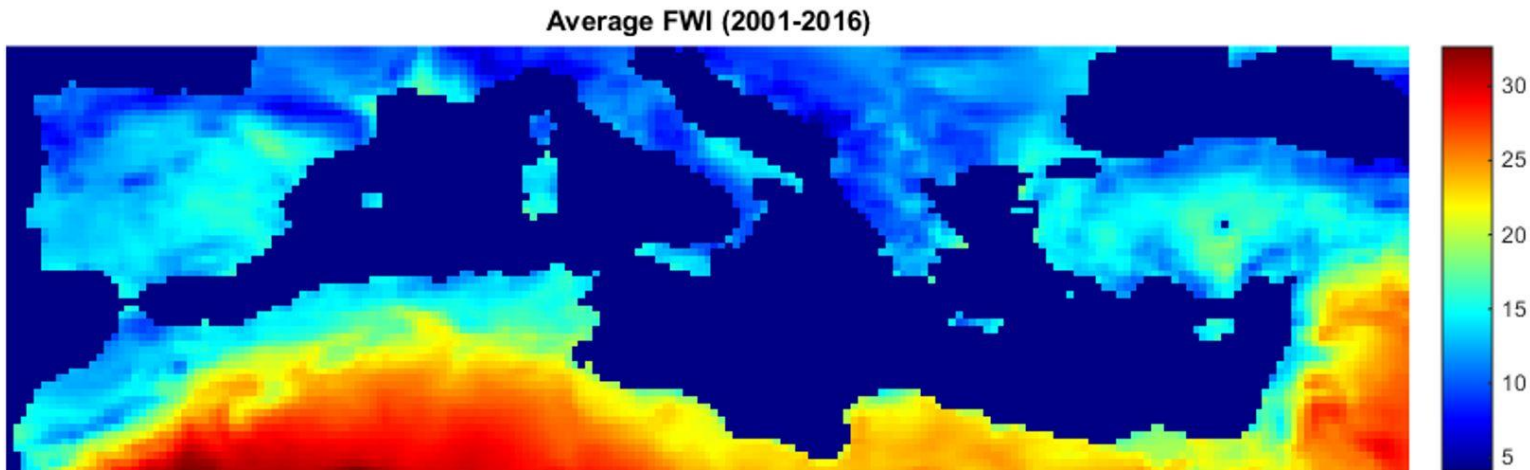


*Figure 12. Fluctuation of the Average FWI values across the Mediterranean Climate Reference Region.*

The areas with the highest average FWI values were mentioned before as the areas with the highest percentages of bare/sparse vegetation. Concluding, that high FWI in these areas does not mean high fire danger.

The first correlation analysis between the monthly BA values and the average monthly FWI values (total of 30,971 set of values) that took place, represents all the grid boxes that experienced Burned Area in the years 2001-2016 and is viewed on Figure 13.

Correlation FWI-logBA

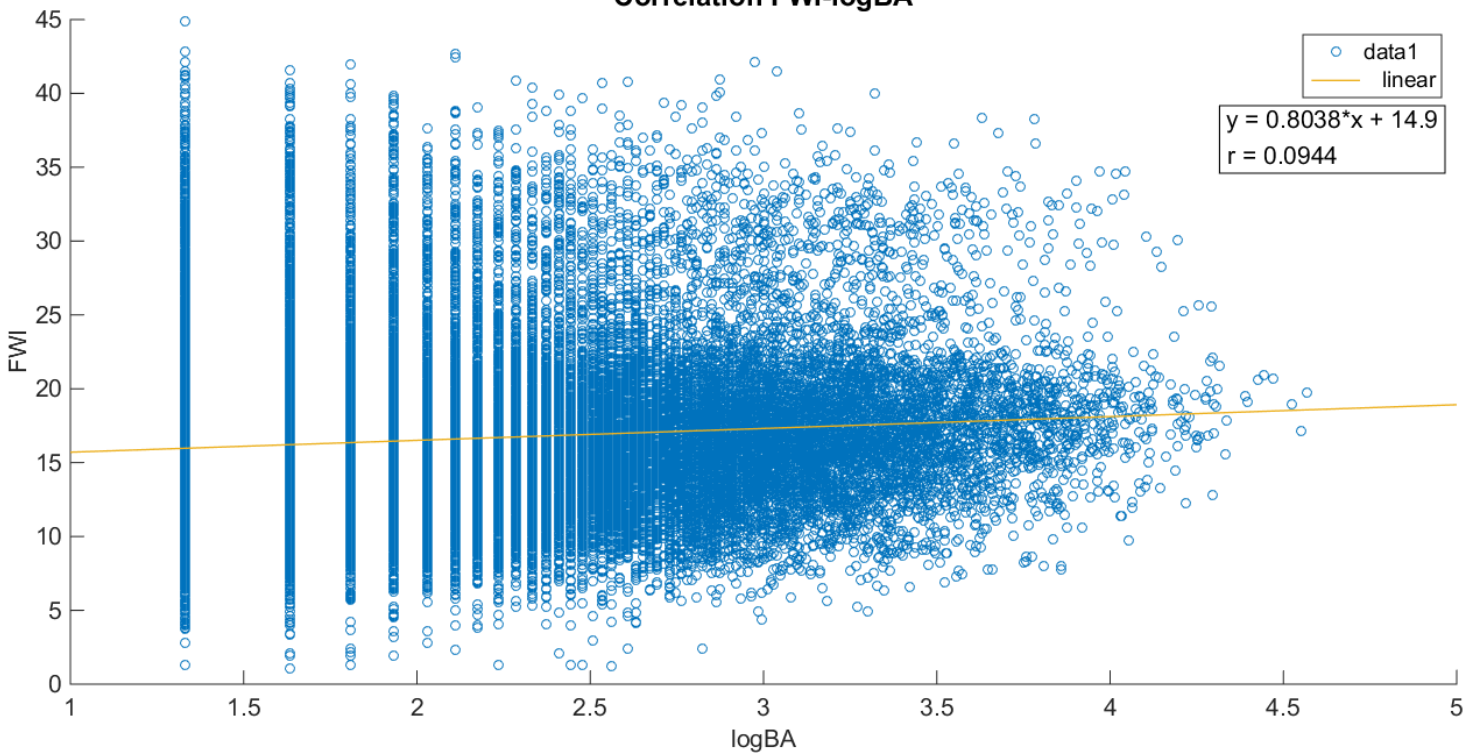


Figure 13. Correlation of the monthly logBA values and the average monthly FWI values.

The Pearson's  $r$  in the above correlation is  $r=0.0944$ , which translates into a very poor positive correlation. It is important here to note, that when looking at the micro level (specific month and specific area), a strong correlation is not expected because high FWI values suggest high fire danger and not high burned area.

For that reason, the set of values were binned into sets of 100 values. In that way, the impact of extreme events, such as a cold winter month with high BA or a warm summer month with low BA, is reduced. By grouping the data into bins, the variability within each bin is reduced, allowing for a clearer representation of the underlying trends in the data.

This can make it easier to identify any patterns or correlations between the FWI and BA values. Additionally, binning can help reduce the noise in the data that may be caused by natural variability or measurement error. This can make it easier to detect and quantify the true underlying relationship between the FWI and BA values. In Figure 14 the correlation between the binned set of values is viewed.

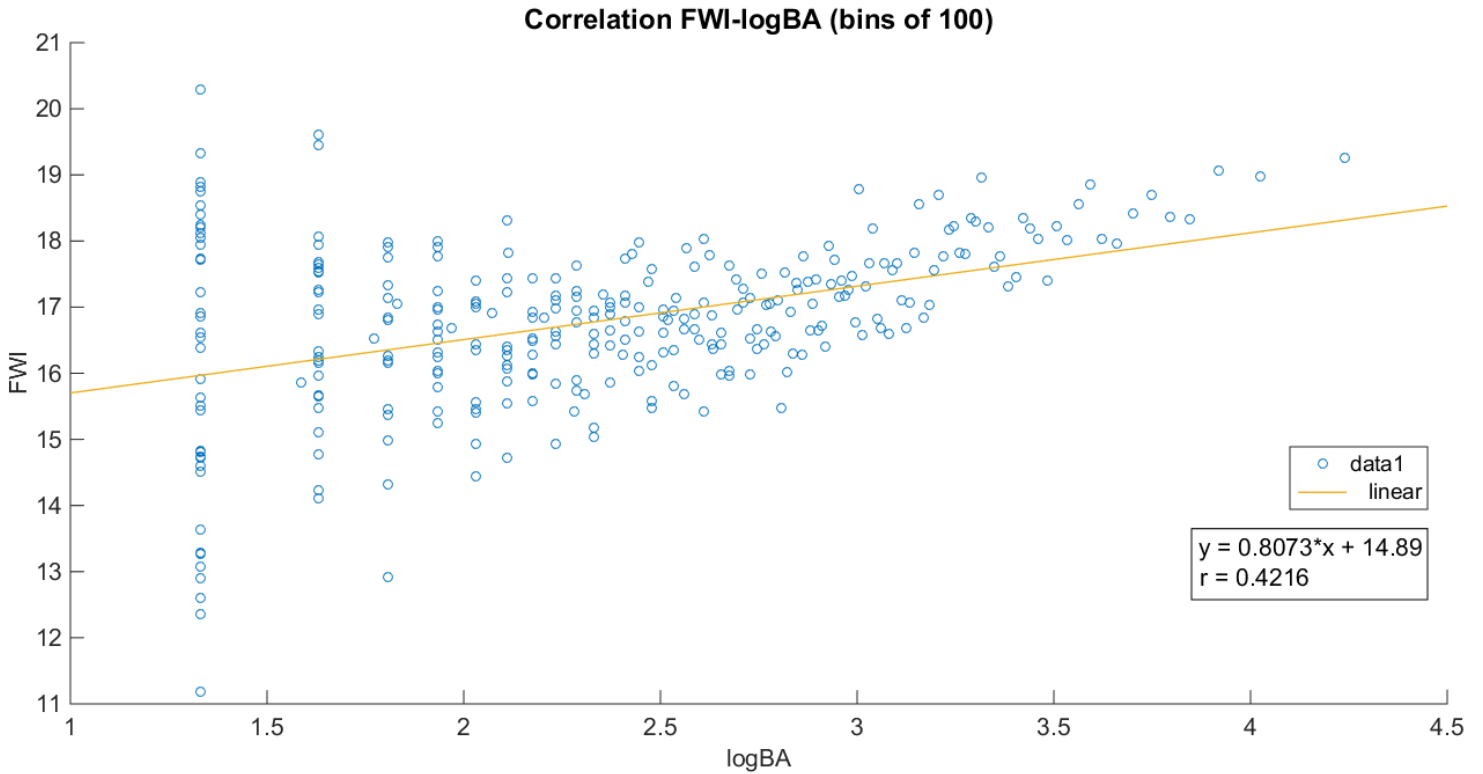


Figure 14. Correlation of the monthly logBA values and the average monthly FWI values (bins of 100).

The Pearson's r in the above correlation is  $r=0.4216$ , which translates into a weak to average positive correlation. Clearly the correlation became much stronger.

Moreover, areas with low values of BA ( $BA < 50$  hectares, or  $\log BA < 1.7$ ) were excluded from the correlation (Figure 15). Firstly, since 21.44 hectares is the lowest value the MODIS satellite can provide as Burned Area, errors or false data might fall on this category. Secondly, because small fires might have started as extreme wildfires, but a quick response from the fire protection agency led to a quick stop of the fire.

Therefore, including these low BA values might bias the analysis and affect the correlation between FWI and BA. Thus, technically the values of 21.44 and 42.87 hectares were the ones excluded from the data. Their corresponding logarithmic values are  $\log(21.44)=1.33$  and  $\log(42.87)=1.63$ .

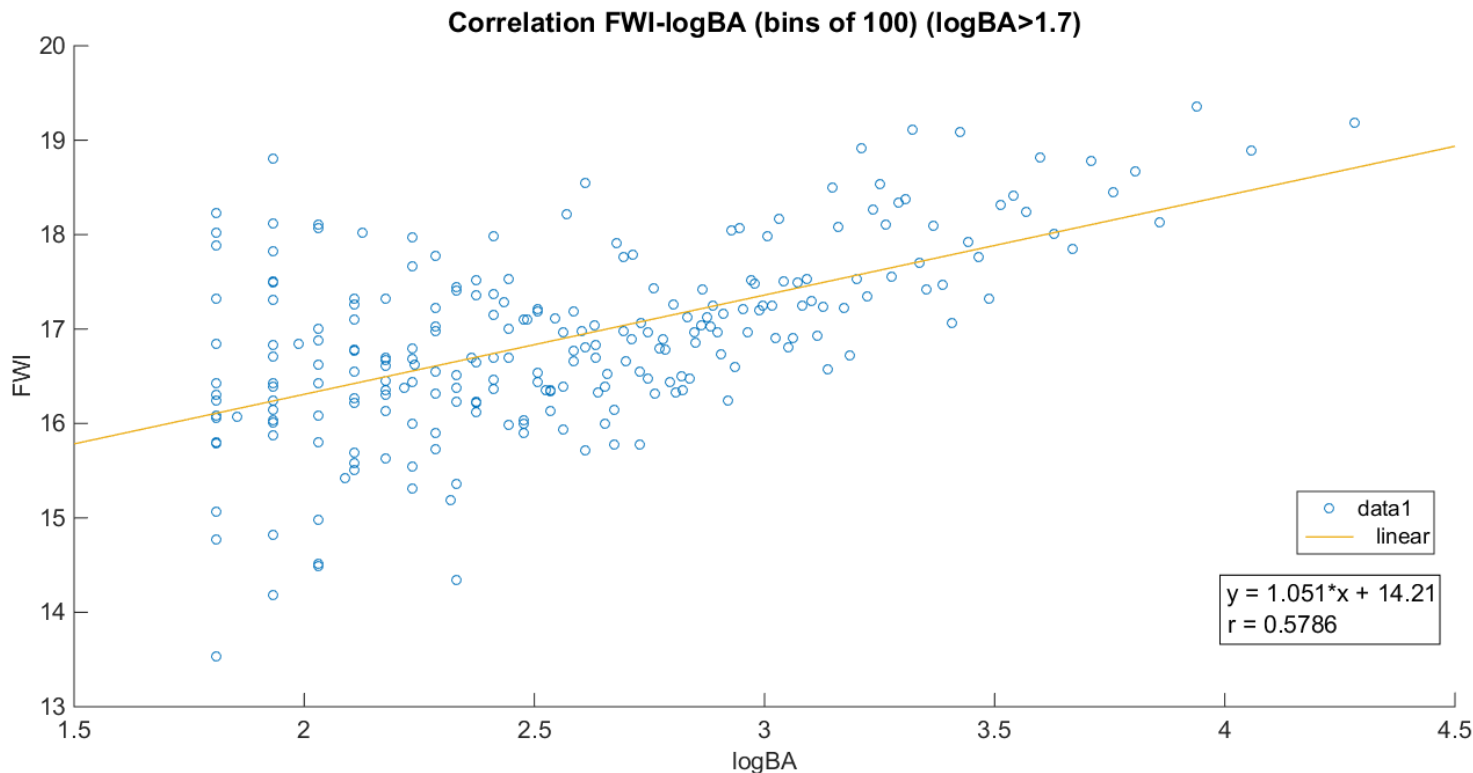


Figure 15. Correlation of the monthly logBA values and the average monthly FWI values (bins of 100) (logBA>1.7).

The Pearson's  $r$  in the above correlation is  $r=0.5786$ , which translates into an average to strong positive correlation. Again, the correlation became stronger following this refinement.

This is a significant improvement compared to the initial correlation before binning the data, which had a Pearson's  $r$  value of only 0.0944. The higher correlation value suggests that binning the data and excluding areas with low BA values may have helped to reduce noise in the data and better capture the relationship between FWI and BA.

The above correlation will be the one to be compared with the experiments of optimization that are provided later in the study.

The second type of correlation, the Correlation Map, can be viewed on Figure 16. The green color represents positive correlation between the two variables (average monthly FWI, monthly logBA) and the red color negative correlation. All the areas with less than 5 months of Burned Area in the study period, were excluded from the correlation.

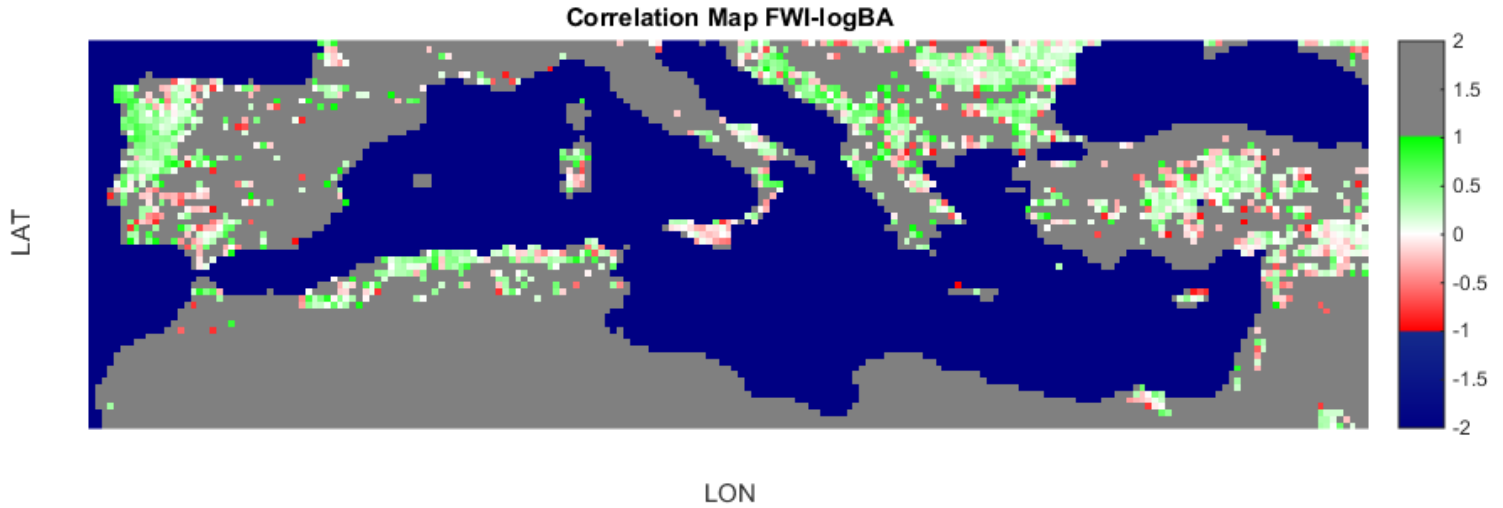


Figure 16. Correlation of the monthly logBA values and the average monthly FWI values on the grid box level ( $\log BA > 1.7$ ) (months of  $BA \geq 5$ ).

In Figure 17, the Correlation Map for the summer months (June-July-August-September – JJAS) of the year can be viewed.

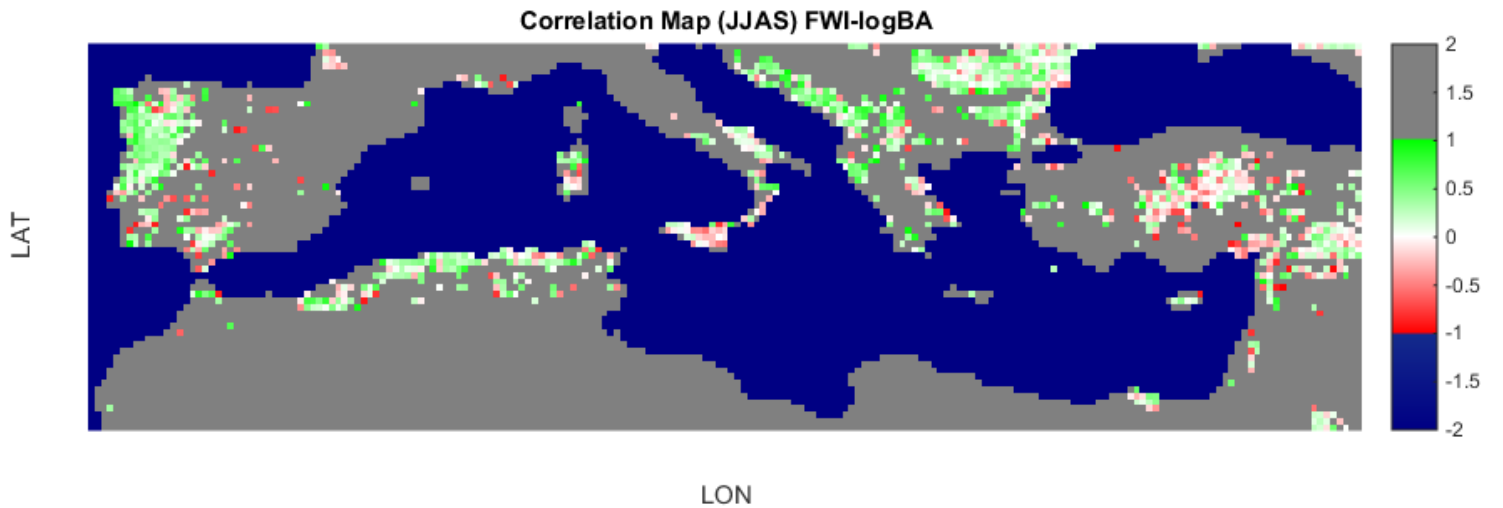


Figure 17. Correlation of the monthly logBA values and the average monthly FWI values on the grid box level ( $\log BA > 1.7$ ) (months of  $BA \geq 5$ ) (JJAS).

Both of the above figures provide mixed correlations throughout the Mediterranean region. More specifically, areas such as Portugal, Northwestern Spain, North Algeria and Tunisia, Croatia up to Albania, Romania and Bulgaria have a mostly positive correlation between the two variables, whereas Turkey, the rest parts of Spain and Syria have a mostly negative correlation.

By comparing Figure 16 and Figure 17 with Figure 11 (Land Cover), the following conclusions are made: Areas with mostly negative correlation are represented by high percentages of cropland and herbaceous type of vegetation. On the other hand, areas with mostly positive correlation are split into two groups. Portugal, Northwestern Spain and Croatia up to Albania are represented by high percentages of forest type of vegetation, whereas North Algeria and Tunisia, Romania and Bulgaria are represented by high percentages of cropland type of vegetation.

The Correlation Maps (Figure 16 and Figure 17) will be used as a comparison for the experiments of optimization that are provided later on the study.

## 5.2. Experiment 1 – FFMC (Ed)

In Figure 18, the Pearson’s  $r$  between the average monthly FWI value and the monthly  $\log BA$ , of all the different sets of  $multip$  and  $expon$  values is viewed for the Experiment 1. It is important to note here that the method of binning the data and excluding areas with low BA is followed in this analysis.

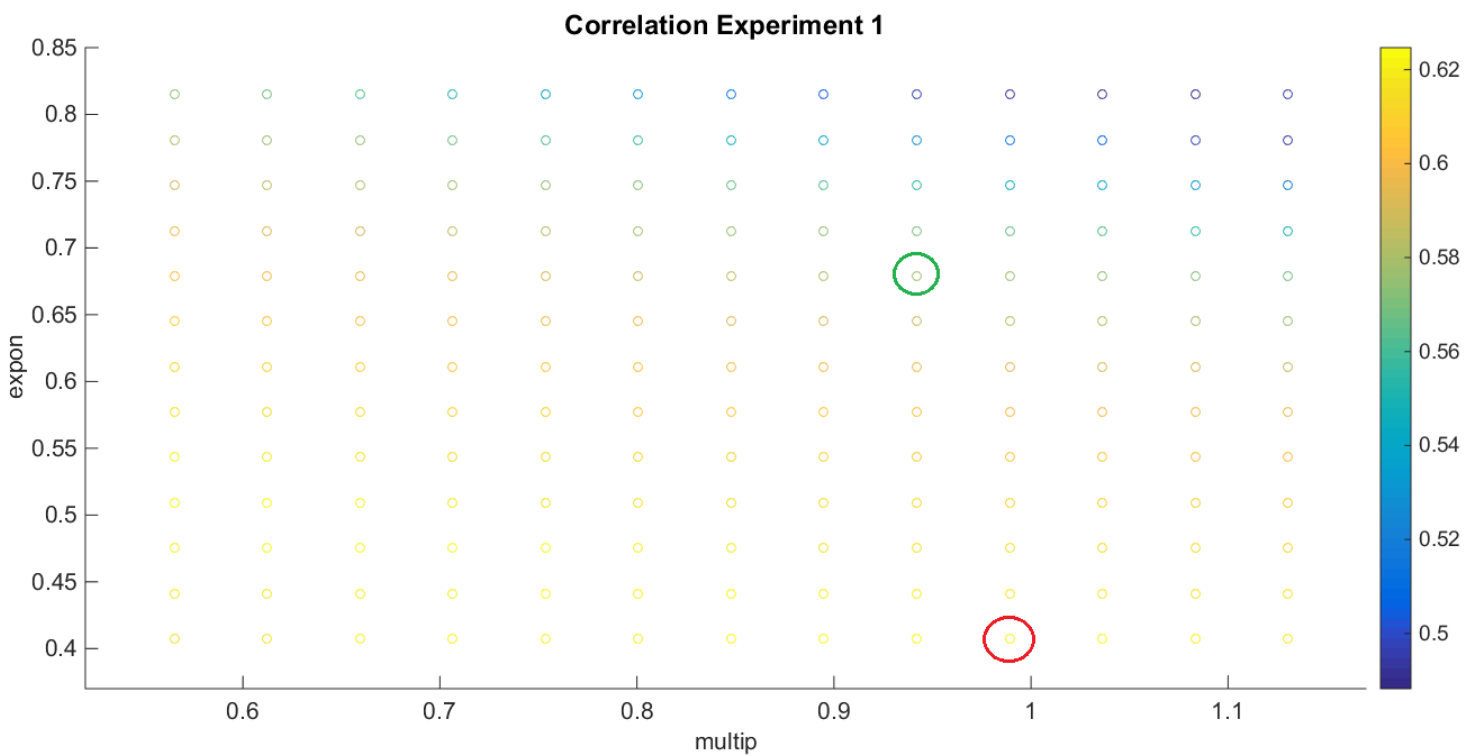


Figure 18. Experiment 1 – Pearson’s  $r$  for all the sets of  $multip$  &  $expon$ .

The green circle represents the Pearson’s  $r$  using the original values of  $multip$  &  $expon$  (original FWI code) with a value of  $r=0.5786$ , whereas the red circle represents the best fit (set of values of  $multip$  &  $expon$  that achieve the highest Pearson’s  $r$ ) of Experiment 1 with a value of  $r=0.6247$ . An increase of about 8%. As a general observation, the Pearson’s  $r$  values tend to get higher as both  $multip$  and  $expon$  decrease. However,  $expon$  seems to have the greatest role in the correlation shifts.

The Correlation Map Difference between the best fit of Experiment 1 and the original code can be viewed on Figure 19.

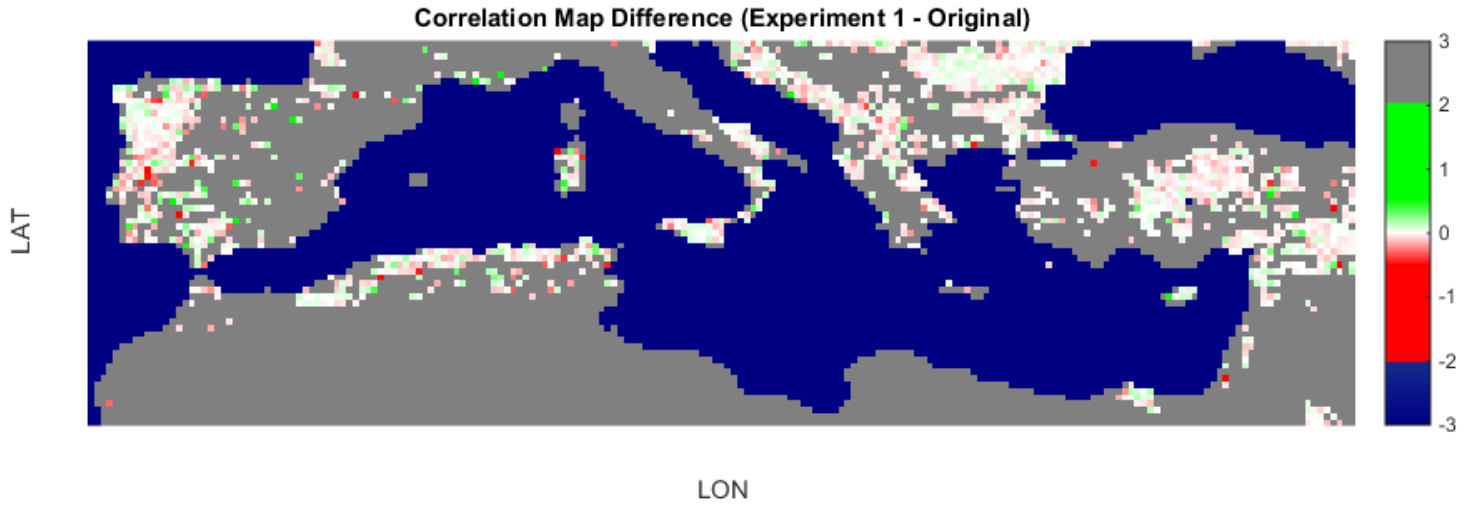


Figure 19. Difference in Pearson's  $r$  between the best fit of Experiment 1 and the original code on the grid box level ( $\log BA > 1.7$ ) (months of  $BA \geq 5$ ).

The Correlation Map Difference for the 4 months (June-July-August-September – JJAS) of the year between the best fit of Experiment 1 and the original code can be viewed on Figure 20.

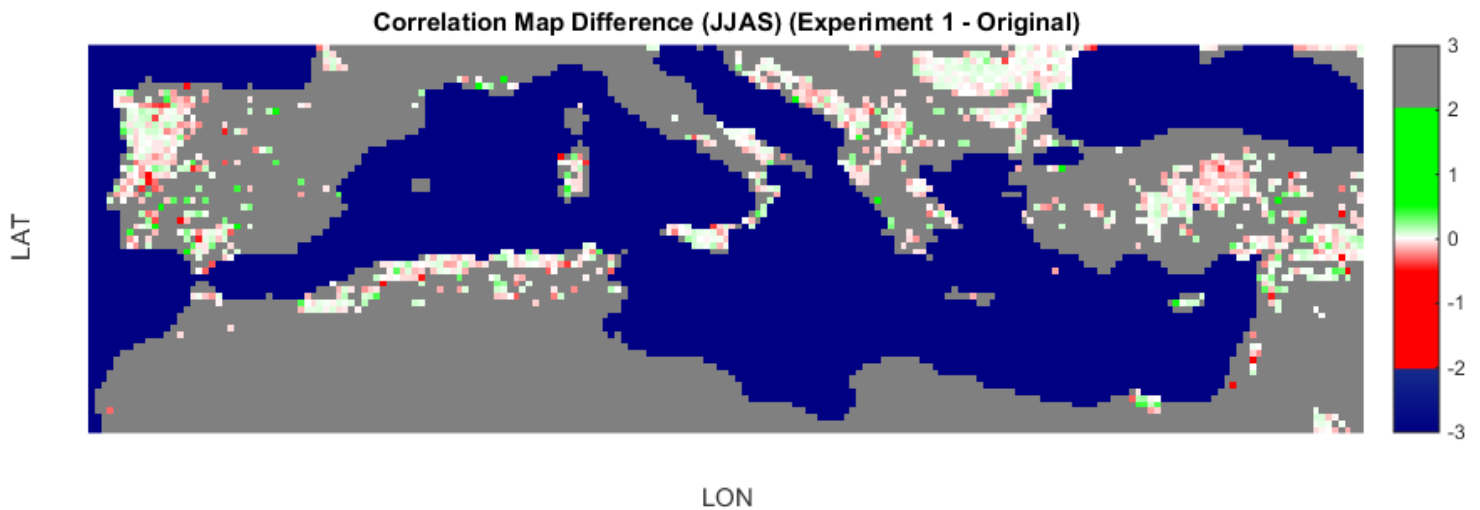


Figure 20. Difference in Pearson's  $r$  between the best fit of Experiment 1 and the original code on the grid box level ( $\log BA > 1.7$ ) (months of  $BA \geq 5$ ) (JJAS).

Even though the overall correlation of the two variables has increased with the use of binning, it is clear from both figures, that there is no trend of overall increase or decrease of the Pearson's  $r$  in any of the individual areas mentioned in the previous paragraph. In this experiment, the spatial diversity in correlation values throughout the region is low.

### 5.3. Experiment 2 – FFMC (Ew)

In Figure 21, the Pearson’s  $r$  between the average monthly FWI value and the monthly logBA, of all the different sets of multip and expon values is viewed of Experiment 2. Again, note here that the method of binning the data and excluding areas with low BA is followed in this correlation.

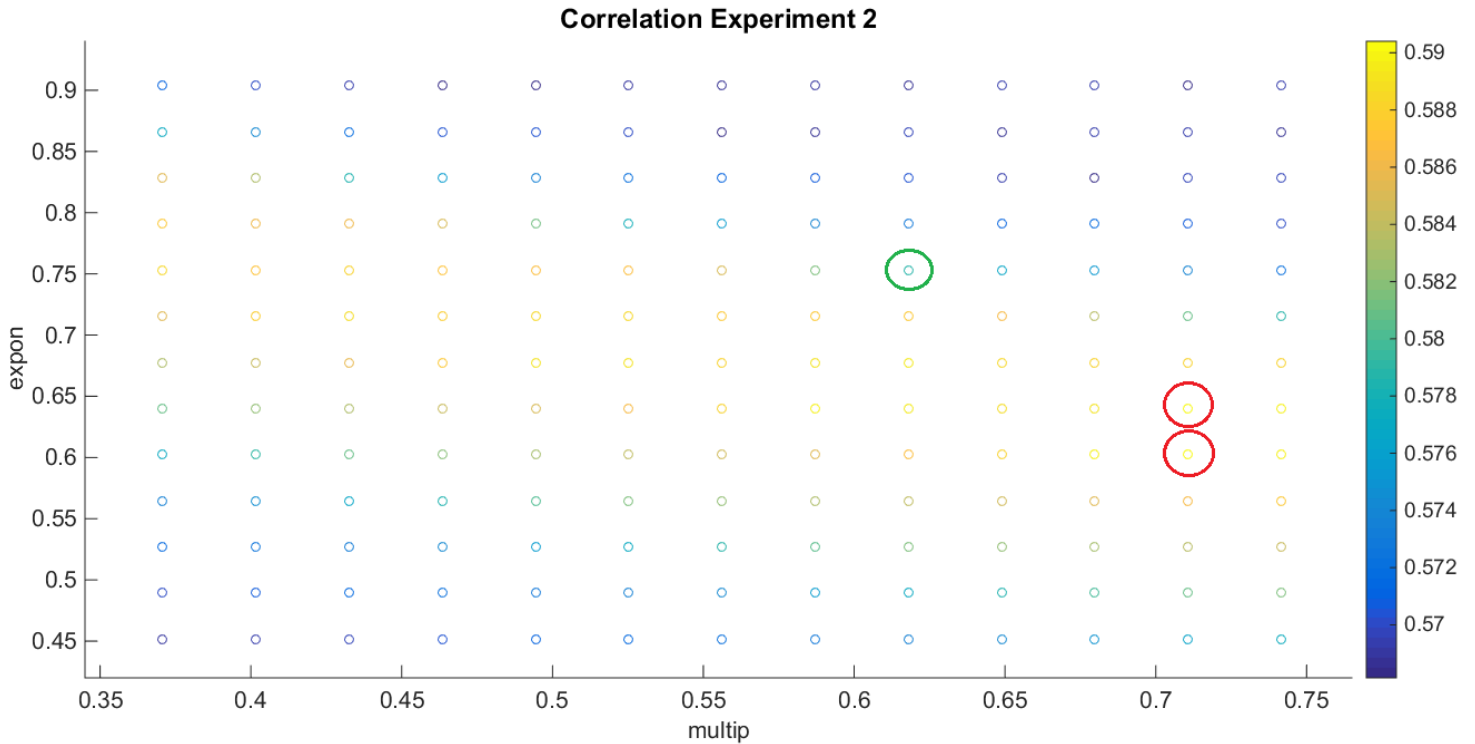


Figure 21. Experiment 2 – Pearson’s  $r$  for all the sets of multip & expon.

The green circle represents the Pearson’s  $r$  using the original values of multip & expon (original FWI code) with a value of  $r=0.5786$ , whereas the red circle represents the best fit (set of values of multip & expon that achieve the highest Pearson’s  $r$ ) of Experiment 1 with a value of  $r=0.5904$ . An increase of about 2%. As we observe on the above Figure, there are two sets of best fit variables, thus the one closest to the original values was kept. As a general observation, the Pearson’s  $r$  has the highest values near the original values of multip and expon, and is kept at similar levels by simultaneously increasing or decreasing the two variables.

The Correlation Map Difference between the best fit of Experiment 2 and the original code can be viewed on Figure 22.

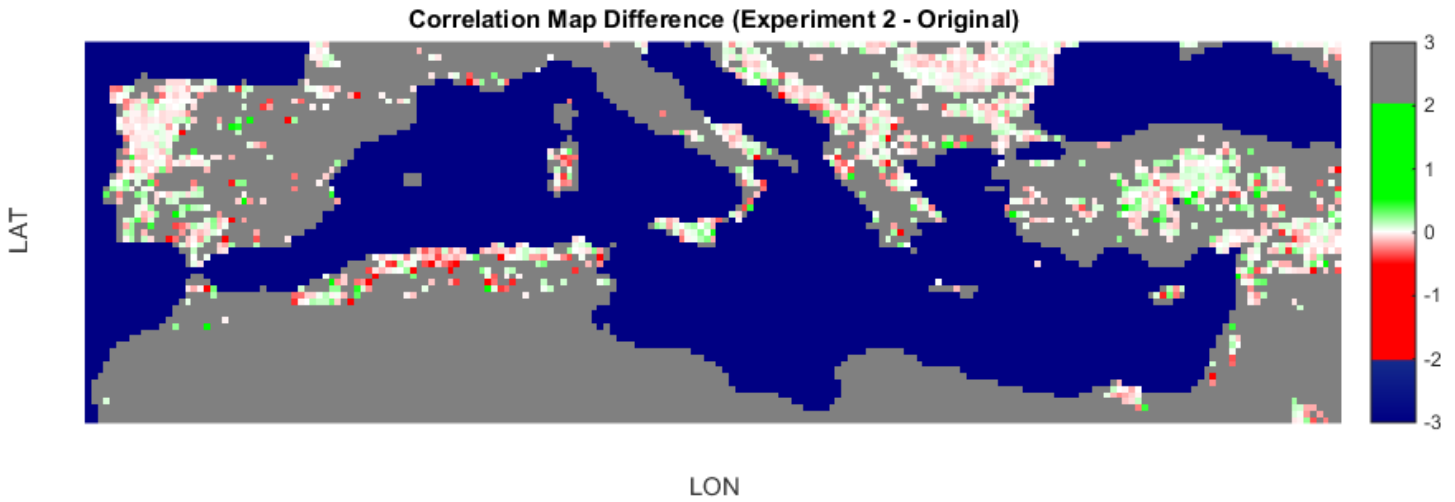


Figure 22. Difference in Pearson's  $r$  between the best fit of Experiment 2 and the original code on the grid box level ( $\log BA > 1.7$ ) (months of  $BA \geq 5$ ).

The Correlation Map Difference for the 4 months (June-July-August-September – JJAS) of the year between the best fit of Experiment 2 and the original code can be viewed on Figure 23.

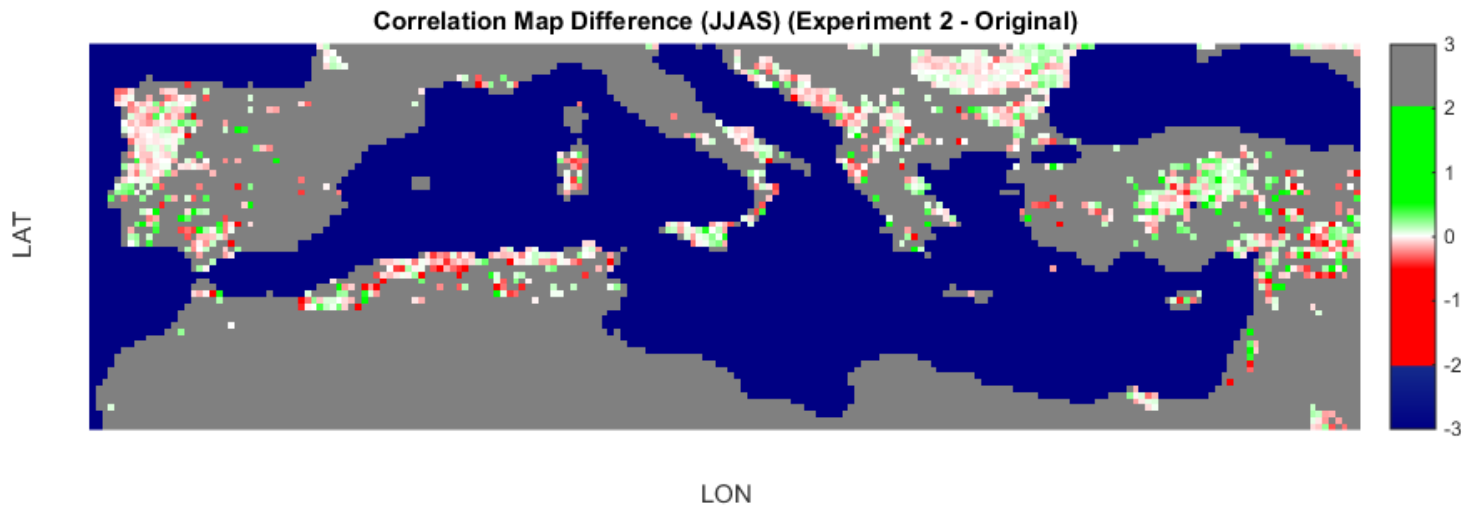


Figure 23. Difference in Pearson's  $r$  between the best fit of Experiment 2 and the original code on the grid box level ( $\log BA > 1.7$ ) (months of  $BA \geq 5$ ) (JJAS).

Even though the overall correlation of the two variables has increased with the use of binning, it is clear from both figures, that there is no trend of overall increase or decrease of the Pearson's  $r$  in any of the individual areas mentioned in the previous paragraph. In this experiment, the spatial diversity in correlation values is higher than in the previous Experiment 1

#### 5.4. Experiment 3 – ISI

In Figure 24 the Pearson's  $r$ , between the average monthly FWI value and the monthly logBA, of all the different sets of  $expon1$  and  $expon2$  values is viewed. Again, note here that the method of binning the data and excluding areas with low BA is followed in this correlation.

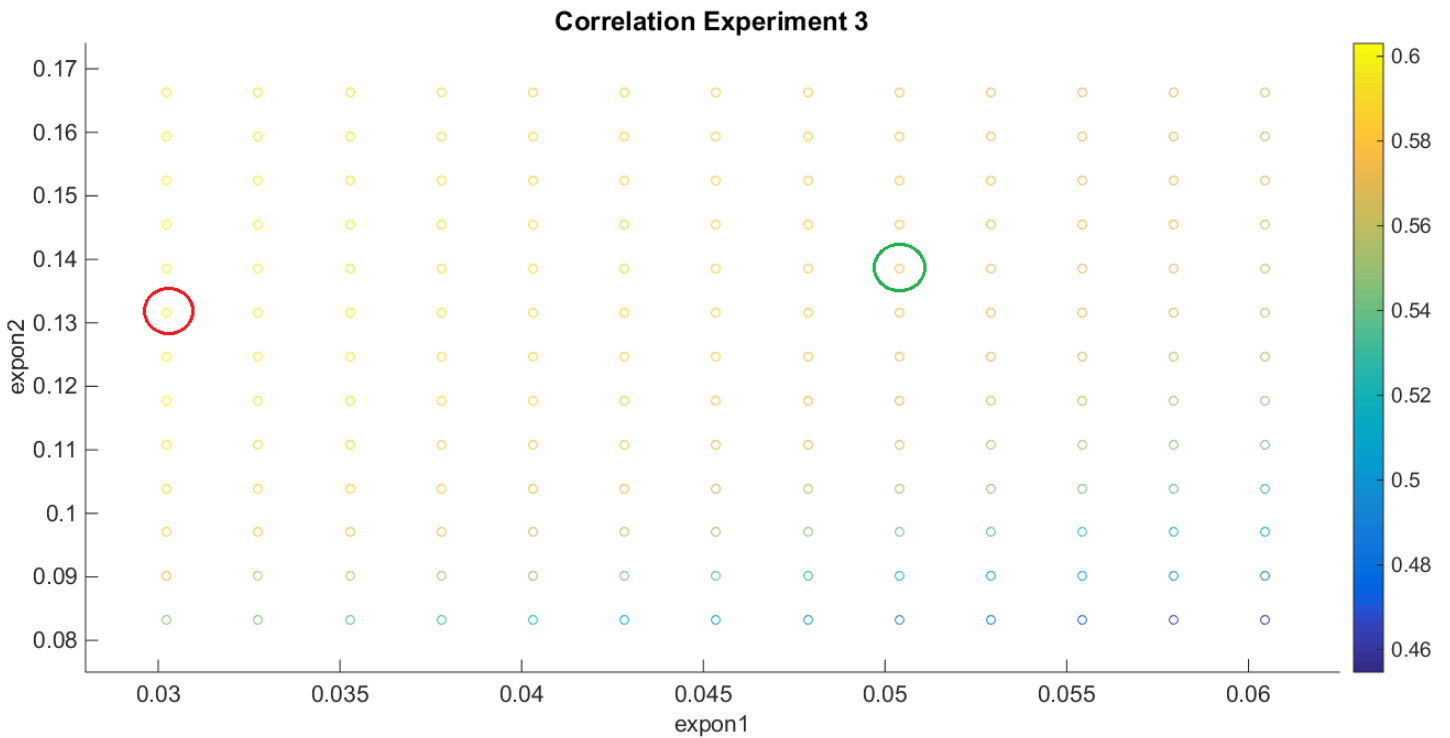


Figure 24. Experiment 3 – Pearson's  $r$  for all the sets of  $expon1$  &  $expon2$ .

The green circle represents the Pearson's  $r$  using the original values of  $expon1$  &  $expon2$  (original FWI code) with a value of  $r=0.5786$ , whereas the red circle represents the best fit (set of values of  $expon1$  &  $expon2$  that achieve the highest Pearson's  $r$ ) of Experiment 3 with a value of  $r=0.6030$ . An increase of about 4%. As a general observation, the Pearson's  $r$  values tend to get higher as  $expon1$  values decrease and  $expon2$  values do not change.  $Expon1$  seems to have the greatest role in the correlation shifts.

The Correlation Map Difference between the best fit of Experiment 3 and the original code can be viewed on Figure 25.

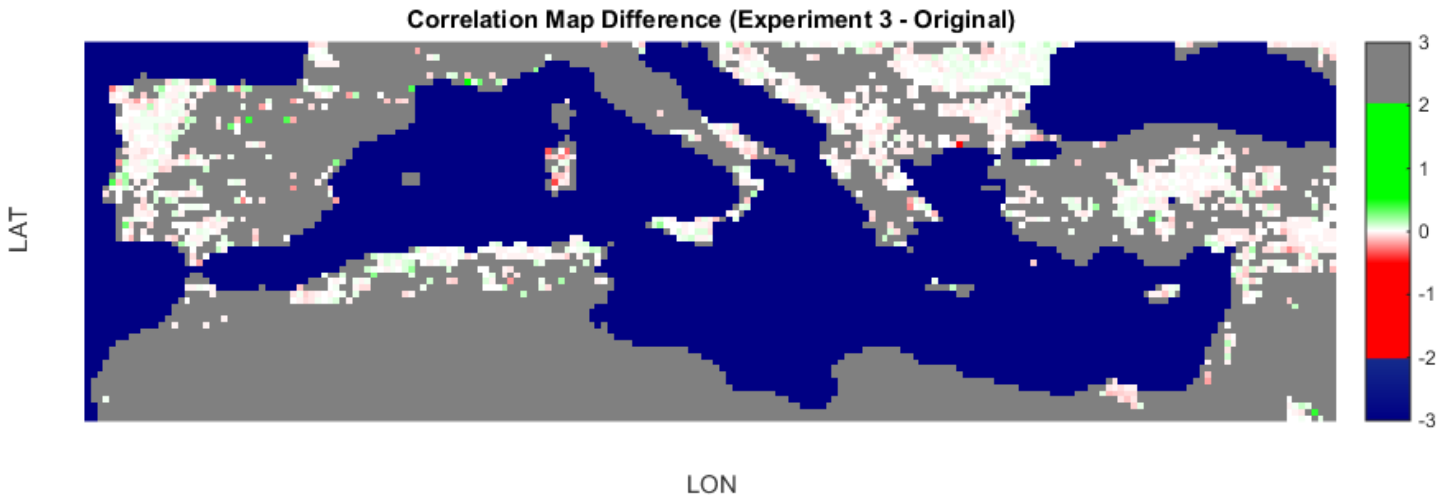


Figure 25. Difference in Pearson's  $r$  between the best fit of Experiment 3 and the original code on the grid box level ( $\log BA > 1.7$ ) (months of  $BA \geq 5$ ).

The Correlation Map Difference for the 4 months (June-July-August-September – JJAS) of the year between the best fit of Experiment 3 and the original code can be viewed on Figure 26.

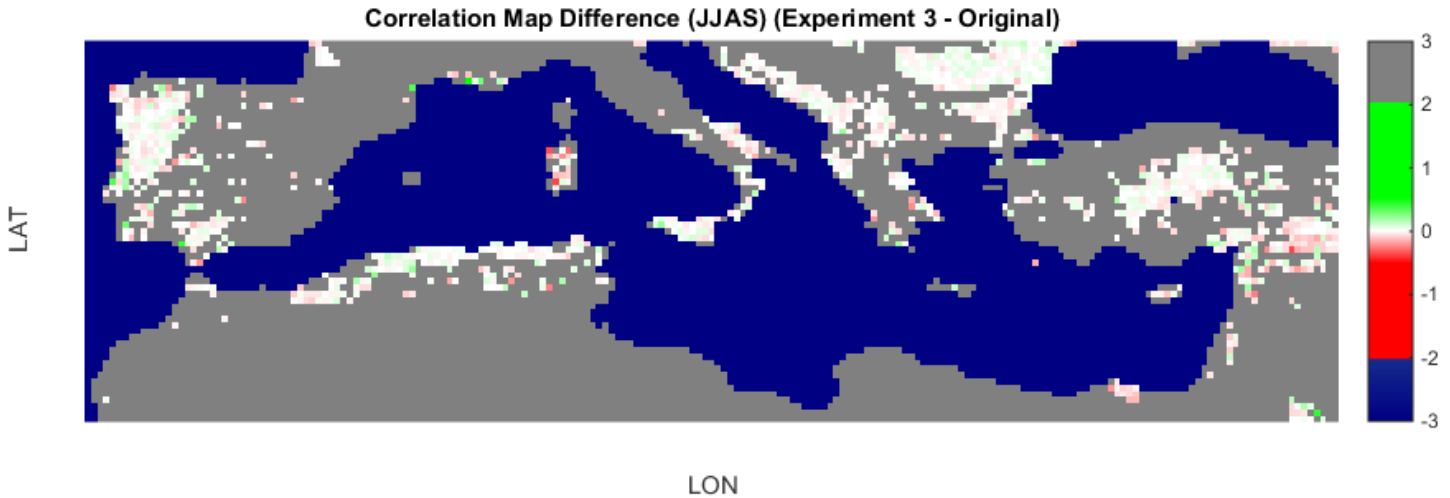


Figure 26. Difference in Pearson's  $r$  between the best fit of Experiment 3 and the original code on the grid box level ( $\log BA > 1.7$ ) (months of  $BA \geq 5$ ) (JJAS).

Even though the overall correlation of the two variables has increased with the use of binning, it is clear from both figures, that there is no trend of overall increase or decrease of the Pearson's  $r$  in any of the individual areas mentioned in the previous paragraph. In this experiment, the spatial diversity in correlation values is lower than both Experiment 1 and Experiment 2.

## 5.5. Experiment 4 – DMC

In Figure 27 the Pearson's  $r$ , between the average monthly FWI value and the monthly logBA, of all the different sets of var1 and var2 values is viewed. Again, note here that the method of binning the data and excluding areas with low BA is followed in this correlation.

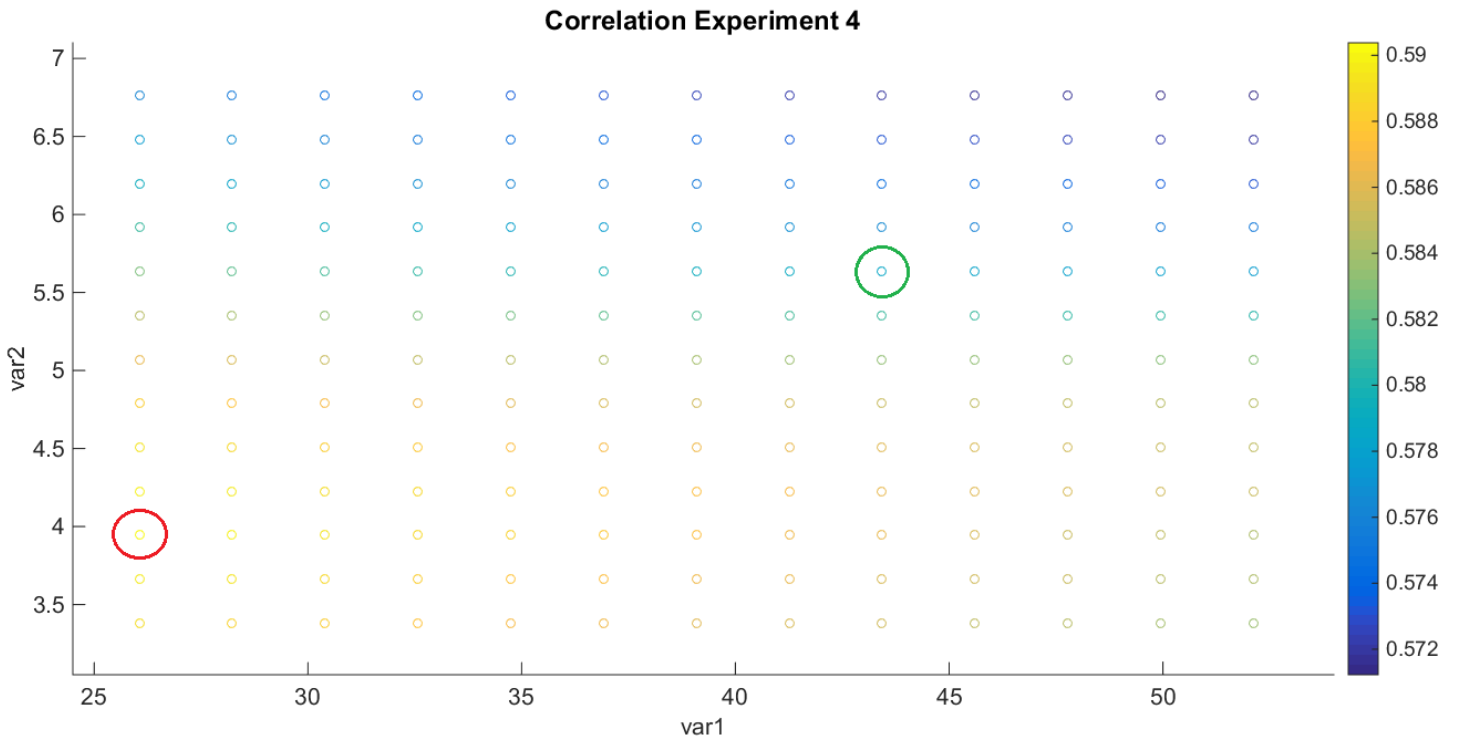


Figure 27. Experiment 4 – Pearson's  $r$  for all the sets of var1 & var2.

The green circle represents the Pearson's  $r$  using the original values of var1 & var2 (original FWI code) with a value of  $r=0.5786$ , whereas the red circle represents the best fit (set of values of var1 & var2 that achieve the highest Pearson's  $r$ ) of Experiment 4 with a value of  $r=0.5904$ . An increase of about 2%. As a general observation, the Pearson's  $r$  values tend to get higher as both var1 and var2 values decrease. Var2 seems to have the biggest role in the correlation shifts.

The Correlation Map Difference between the best fit of Experiment 4 and the original code can be viewed on Figure 28.

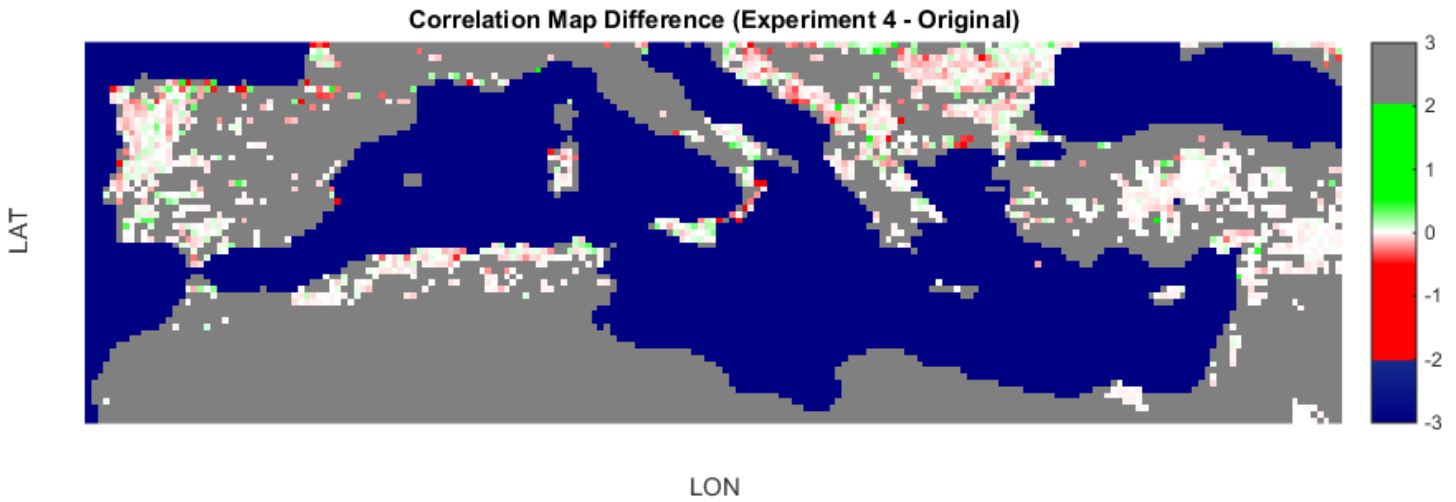


Figure 28. Difference in Pearson's  $r$  between the best fit of Experiment 4 and the original code on the grid box level ( $\log BA > 1.7$ ) (months of  $BA \geq 5$ ).

The Correlation Map Difference for the 4 months (June-July-August-September – JJAS) of the year between the best fit of Experiment 4 and the original code can be viewed on Figure 29.

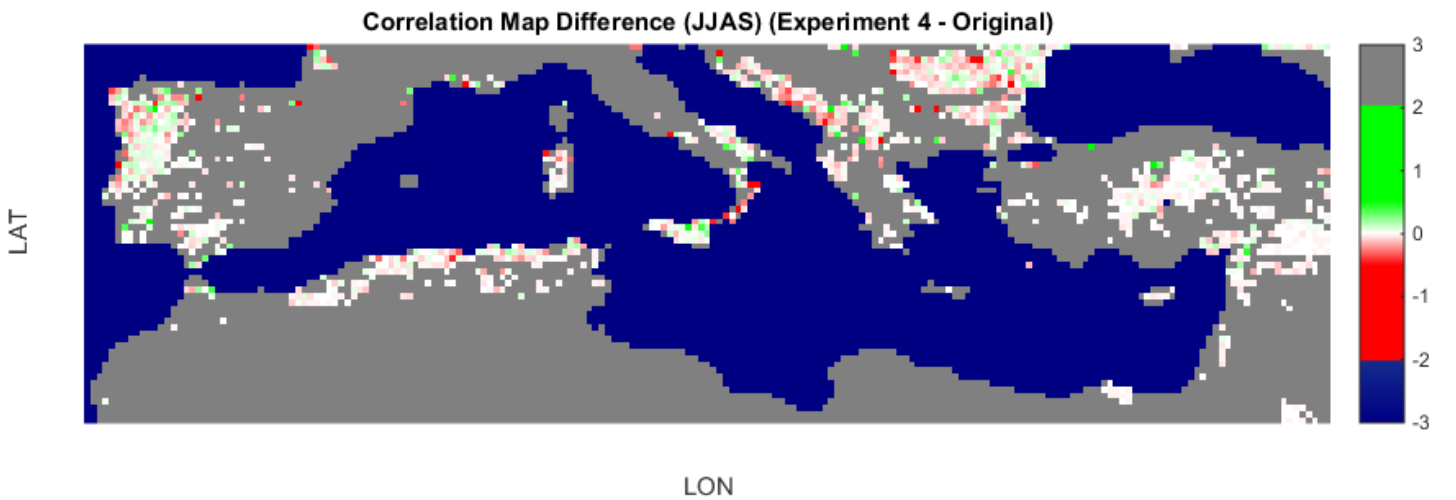


Figure 29. Difference in Pearson's  $r$  between the best fit of Experiment 4 and the original code on the grid box level ( $\log BA > 1.7$ ) (months of  $BA \geq 5$ ) (JJAS).

Even though the overall correlation of the two variables has increased with the use of binning, it is clear from both figures, that there is no trend of overall increase or decrease of the Pearson's  $r$  in any of the individual areas mentioned in the previous paragraph. In this experiment, the spatial diversity in correlation values is similar to Experiment 1.

## 5.6. Combinations

From the results of the previous Experiments, it is clear that the FWI code can actually be improved in terms of predicting Burned Area by altering certain constants of its equations.

In the next and final step, combinations of the above Experiments were run, using the values that provided the best fit for the constants from each Experiment. The combinations with the best results are presented subsequently.

### 5.6.1. Combination 1-2-3

Combination 1-2-3, incorporates the best fit alterations of Experiment 1, Experiment 2 and Experiment 3, that yielded the highest Pearson's  $r$  in each Experiment. In Figure 30, the correlation of the two variables is viewed.

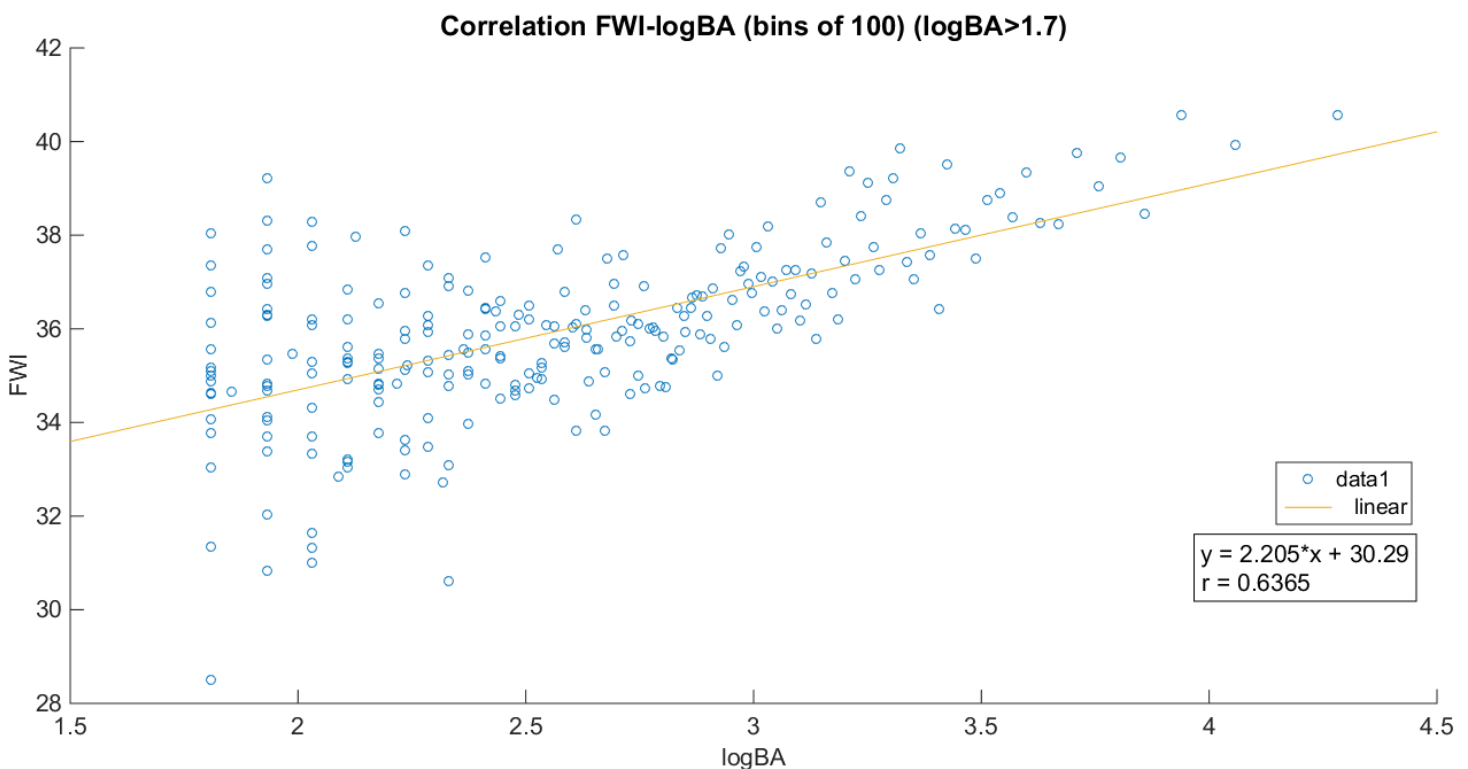


Figure 30. Correlation of the monthly logBA values and the average monthly FWI values (bins of 100) (logBA>1.7) (Combination 1-2-3).

The highest Pearson's  $r$  of Combination 1-2-3 has a value of  $r=0.6365$ , which shows an increase of about 10% compared to the Pearson's  $r$  of the original code. An important observation is that the FWI values range from 28 to 42, compared to Figure 16, where they ranged from 13 to 20.

The Correlation Map Difference between the Combination 1-2-3 and the original code can be viewed in Figure 31.

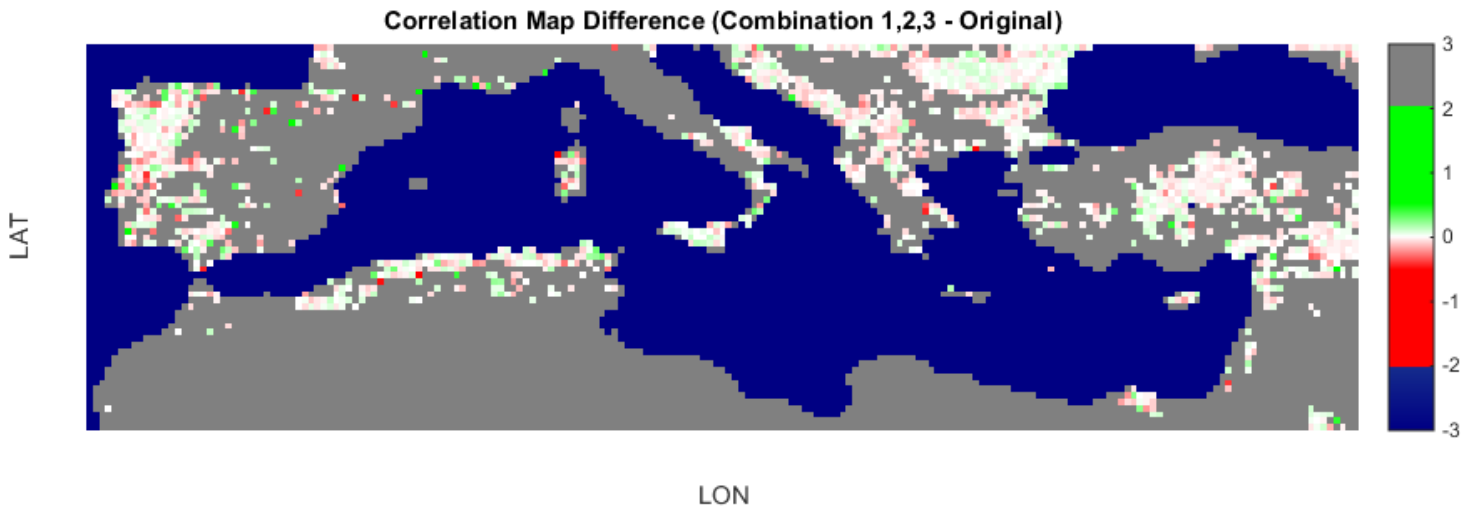


Figure 31. Difference in Pearson's  $r$  between Combination 1-2-3 and the original code on the grid box level ( $\log BA > 1.7$ ) (months of  $BA \geq 5$ ).

The Correlation Map Difference for the 4 months (June-July-August-September – JJAS) of the year between the best fit of Combination 1-2-3 and the original code can be viewed on Figure 32.

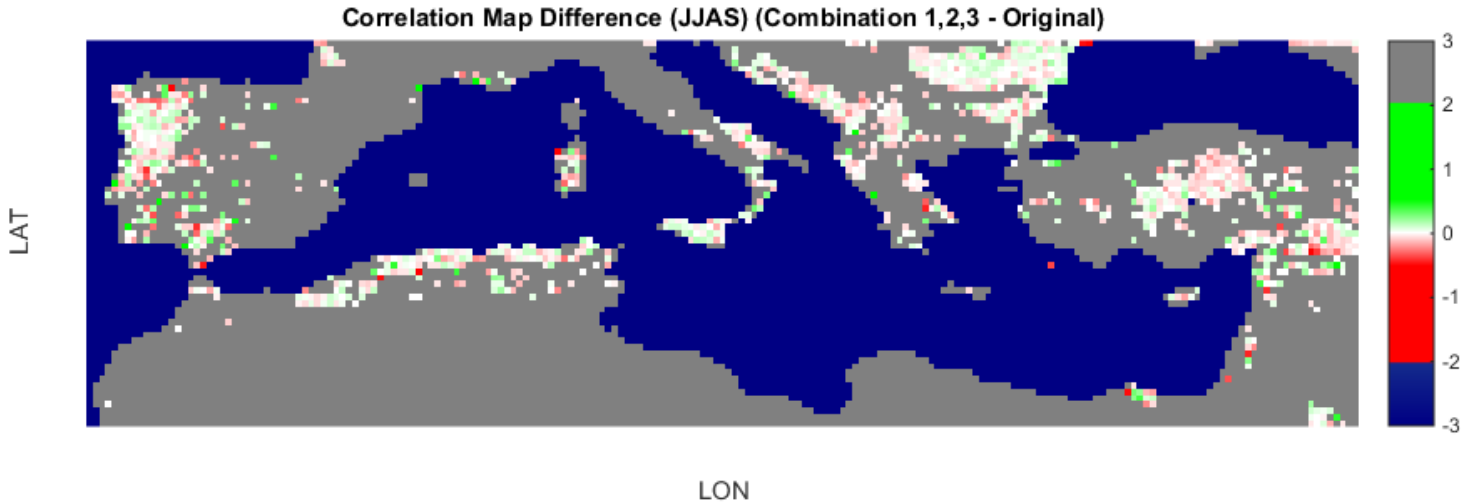


Figure 32. Difference in Pearson's  $r$  between Combination 1-2-3 and the original code on the grid box level ( $\log BA > 1.7$ ) (months of  $BA \geq 5$ ) (JJAS).

Again, the overall correlation of the two variables has increased with the use of binning, however, it is clear from both figures, that there is no trend of overall increase or decrease of the Pearson's  $r$ . Mostly small differences in correlation values are observed throughout the region. The spatial diversity of correlation values is similar to that from Experiment 1.

### 5.6.2. Combination 1-2-3-4

Combination 1-2-3-4, incorporates the best fit alterations of Experiment 1, Experiment 2, Experiment 3 and Experiment 4 that yielded the highest Pearson's  $r$  in each Experiment. In Figure 33, the correlation of the two variables is viewed.

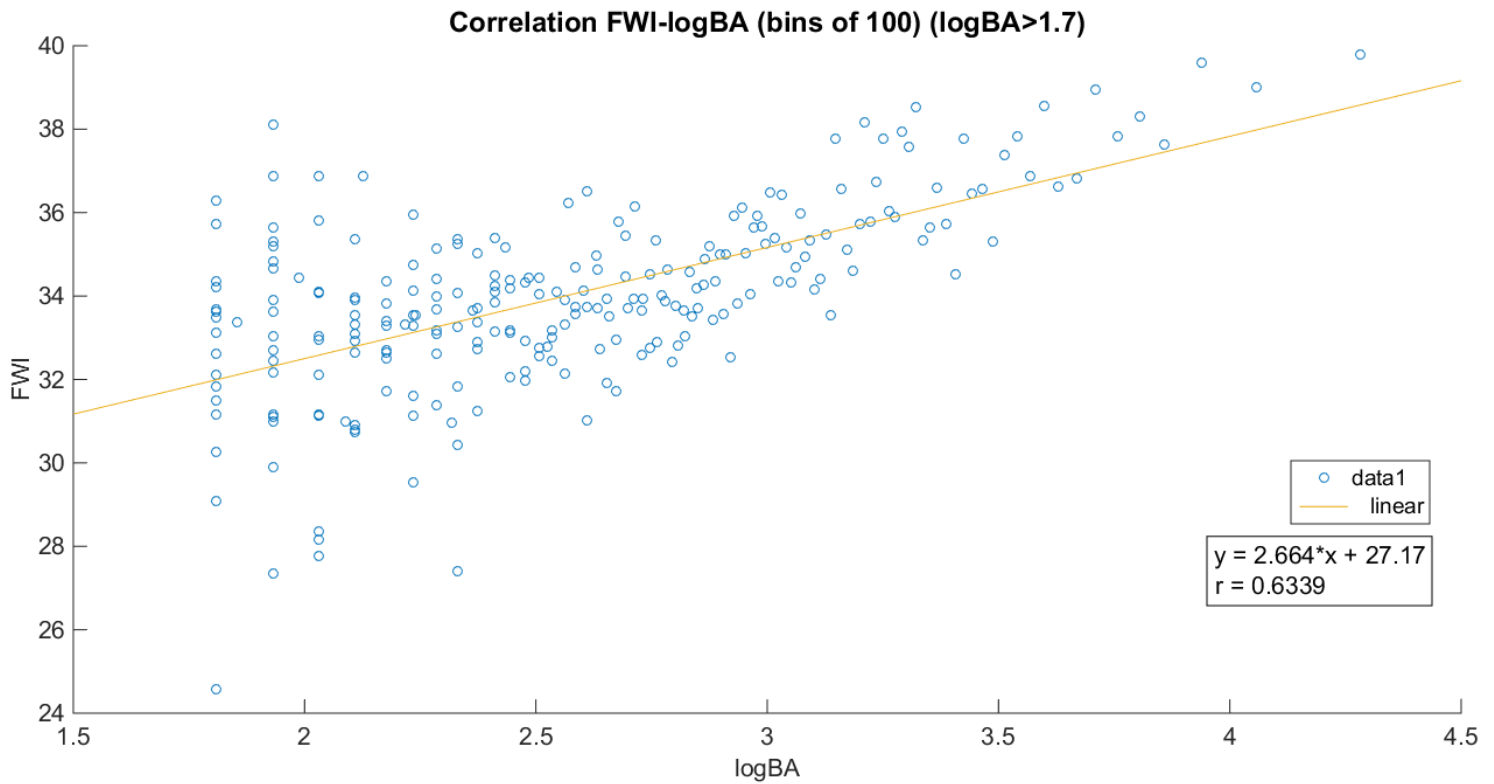


Figure 33. Correlation of the monthly logBA values and the average monthly FWI values (bins of 100) (logBA>1.7), (Combination 1-2-3-4).

The highest Pearson's  $r$  of Combination 1-2-3-4 has a value of  $r=0.6339$ , which shows an increase of about 9,5% compared to the Pearson's  $r$  of the original code. An important observation is the FWI values, ranging from 24 to 40, compared to Figure 16, ranging from 13 to 20.

The Correlation Map Difference between the best fit of Combination 1-2-3-4 and the original code can be viewed on Figure 34.

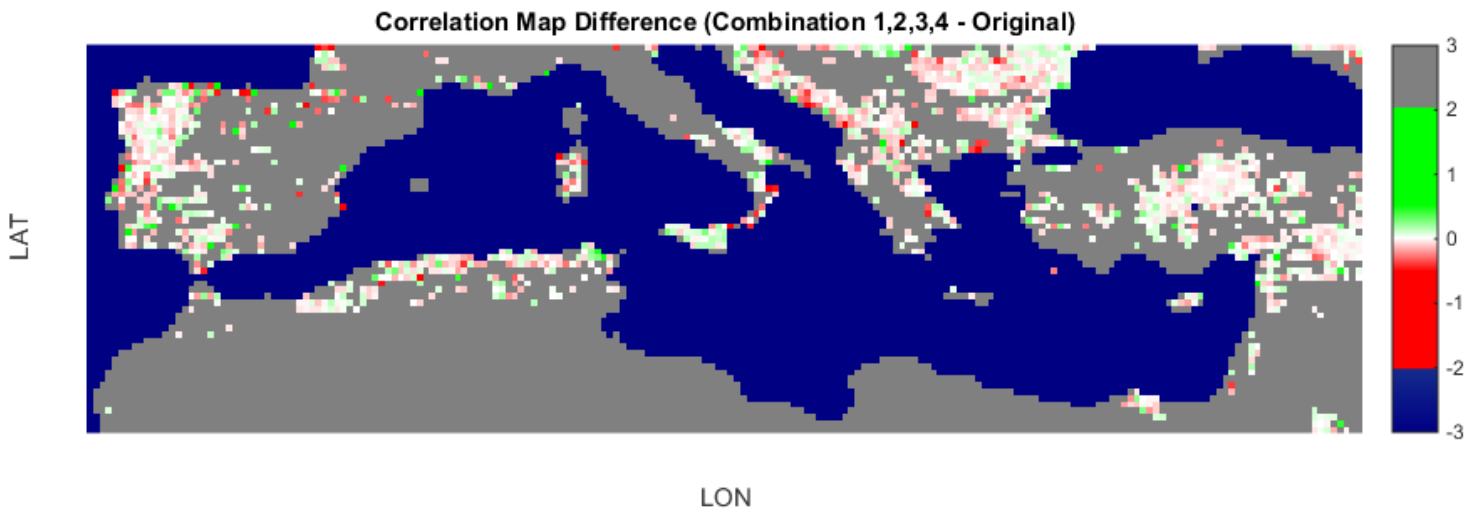


Figure 34. Difference in Pearson's  $r$  between Combination 1-2-3-4 and the original code on the grid box level ( $\log BA > 1.7$ ) (months of  $BA \geq 5$ ).

The Correlation Map Difference for the 4 months (June-July-August-September – JJAS) of the year between the best fit of Combination 1-2-3-4 and the original code can be viewed on Figure 35.

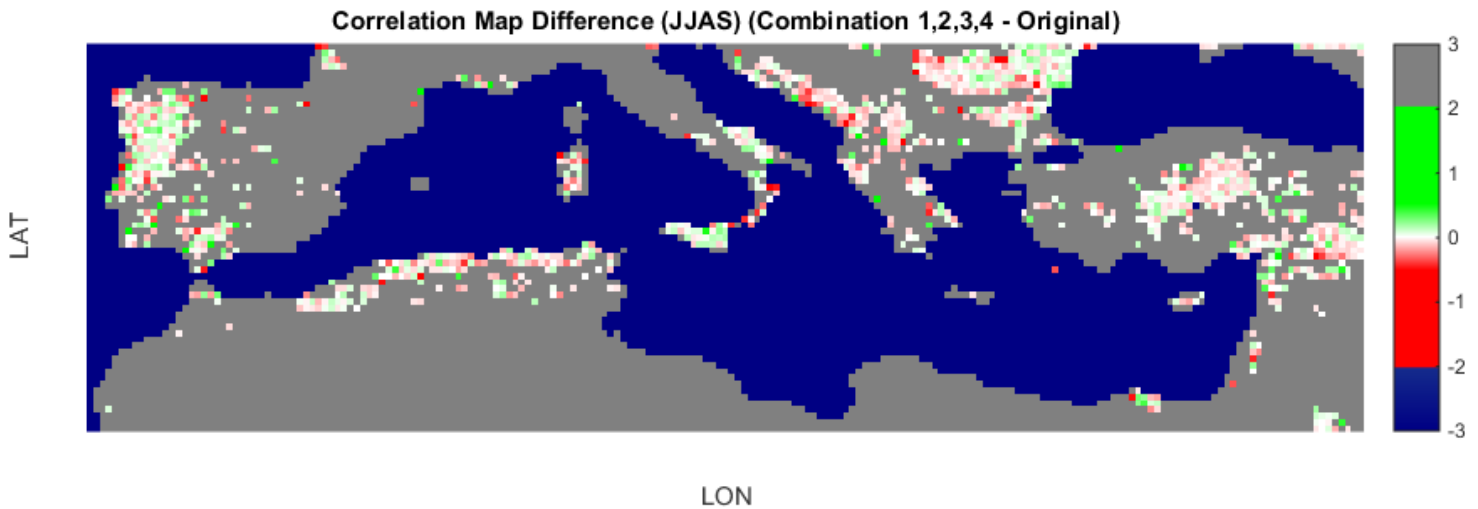


Figure 35. Difference in Pearson's  $r$  between Combination 1-2-3-4 and the original code on the grid box level ( $\log BA > 1.7$ ) (months of  $BA \geq 5$ ) (JJAS).

Again, the overall correlation of the two variables has increased with the use of binning, however, it is clear from both figures, that there is no trend of overall increase or decrease of the Pearson's  $r$ . Mostly small differences in correlation values are observed throughout the region. The spatial diversity of correlation values is similar to that from Experiment 4.

### 5.6.3. Combination 3-4

Combination 3-4, incorporates the best fit alterations of Experiment 3 and Experiment 4, that yielded the highest Pearson's  $r$  in each Experiment. In Figure 36, the correlation of the two variables is viewed.

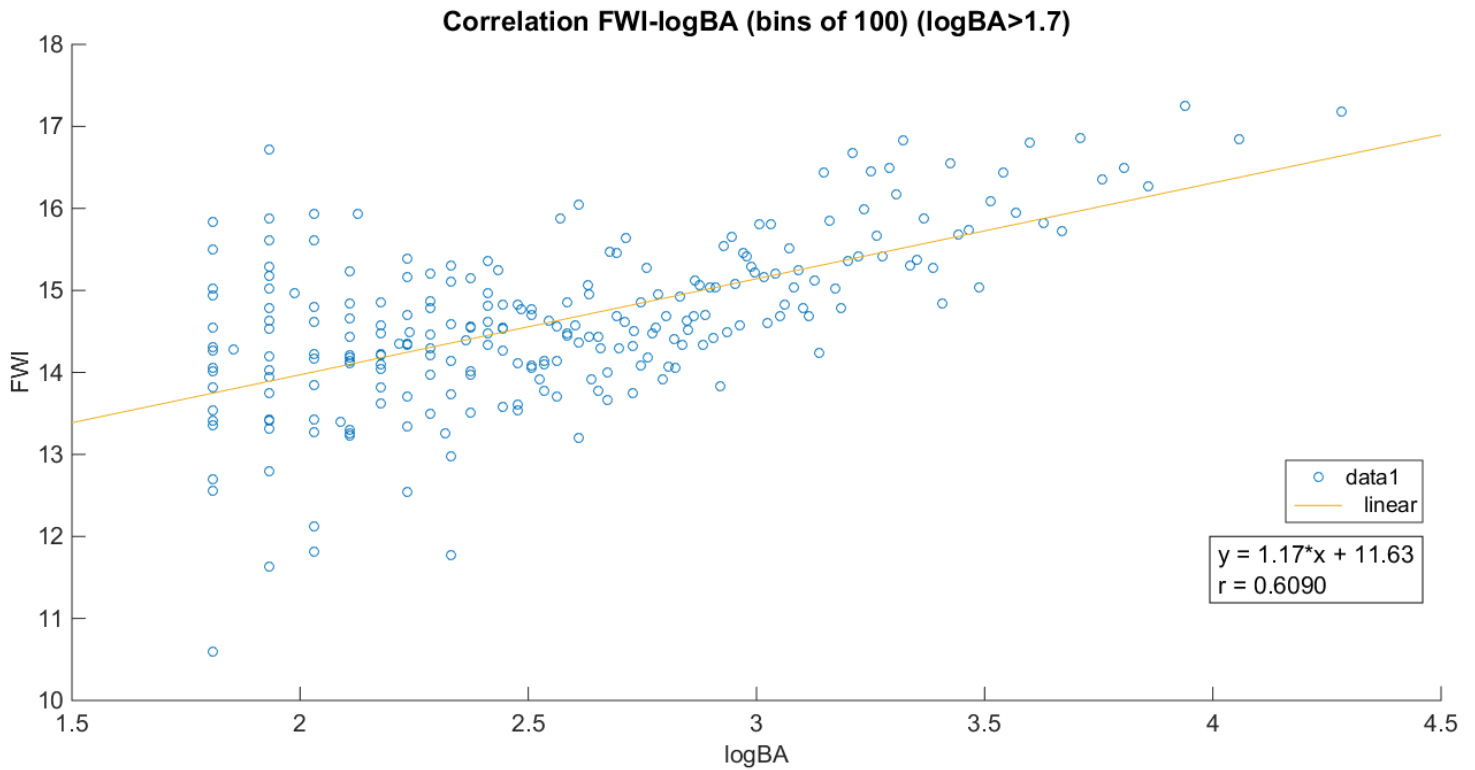


Figure 36. Correlation of the monthly logBA values and the average monthly FWI values (bins of 100) (logBA>1.7), (Combination 3-4).

The highest Pearson's  $r$  of Combination 3-4 has a value of  $r=0.6090$ , which shows an increase of about 5% compared to the Pearson's  $r$  of the original code. An important observation is the FWI values, ranging from 10 to 18, compared Figure 16, ranging from 13 to 20.

The Correlation Map Difference between the best fit of Combination 3-4 and the original code can be viewed on Figure 37.

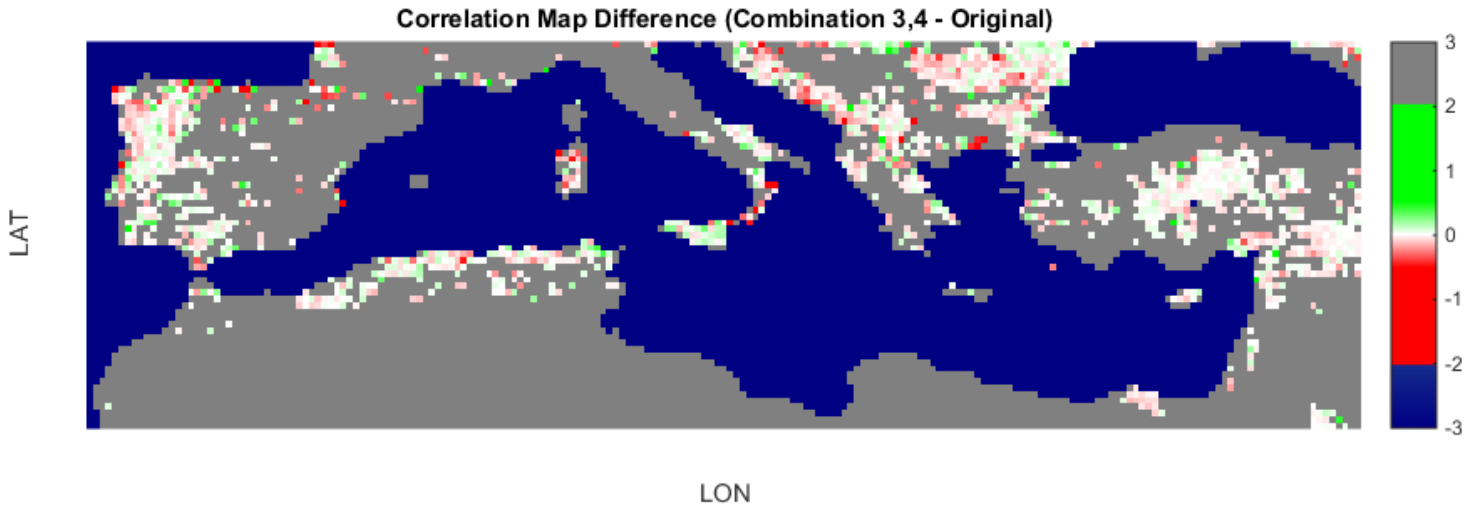


Figure 37. Difference in Pearson's  $r$  between Combination 3-4 and the original code on the grid box level ( $\log BA > 1.7$ ) (months of  $BA \geq 5$ ).

The Correlation Map Difference for the 4 months (June-July-August-September – JJAS) of the year between the best fit of Combination 3-4 and the original code can be viewed on Figure 38.

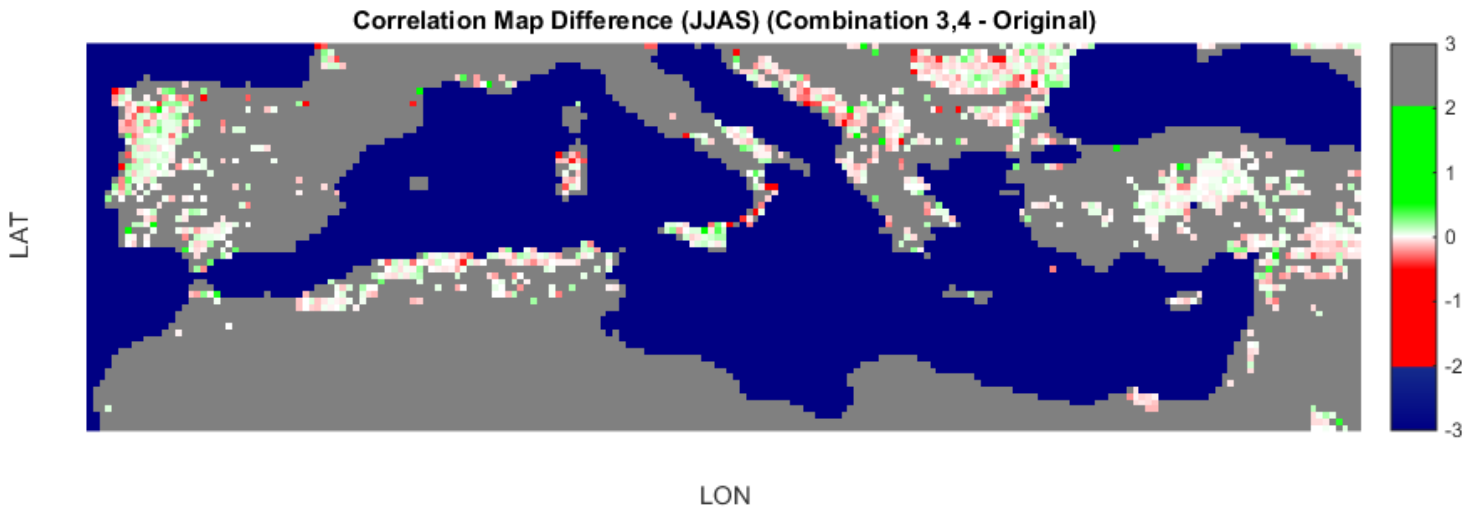


Figure 38. Difference in Pearson's  $r$  between Combination 3-4 and the original code on the grid box level ( $\log BA > 1.7$ ) (months of  $BA \geq 5$ ) (JJAS).

Again, the overall correlation of the two variables has increased with the use of binning, however, it is clear from both figures that there is no trend of overall increase or decrease of the Pearson's  $r$ . Mostly small differences in correlation values are observed throughout the region. The spatial diversity of correlation values is similar to that from Experiment 4.

## 6. Discussion

This study shows that an underlying positive correlation exists between the monthly average FWI values and the logBA values, by using the method of data binning and excluding low values of BA.

From the first method of correlation (all the grid boxes of the study region with Burned Area data), the Experiments and their Combinations suggest, that this correlation can actually get stronger by altering certain constants of the FWI equations. More specifically the increases in Pearson's  $r$  are:

- Experiment 1:  $r=0.5786 \rightarrow r=0.6247$  (8% increase)
- Experiment 2:  $r=0.5786 \rightarrow r=0.5904$  (2% increase)
- Experiment 3:  $r=0.5786 \rightarrow r=0.6030$  (4% increase)
- Experiment 4:  $r=0.5786 \rightarrow r=0.5904$  (2% increase)
- Combination 1-2-3:  $r=0.5786 \rightarrow r=0.6365$  (10% increase)
- Combination 1-2-3-4:  $r=0.5786 \rightarrow r=0.6339$  (9.5% increase)
- Combination 3-4:  $r=0.5786 \rightarrow r=0.6090$  (5% increase)

As seen on the above list, the correlation of the two variables can increase, depending on the alterations made on the FWI equations, thus improving the FWI in predicting possible wildfire events in this study. However, from Figures 31, 34 and 37, it is observed that even though the goal of increased correlation is achieved, the values of average FWI vary substantially from the corresponding values of the original FWI code. Specific attention should be paid to this observation, since certain values of FWI are associated with certain fire risk thresholds for different regions, e.g. in Karali et al. (2014) these thresholds are established for Greece.

On the other hand, from the second type of correlation, on the grid box level (Correlation Map & Correlation Map Difference), no pattern of increase or decrease in correlation was observed, throughout the study region. This probably happens due to the fact that many grid boxes were excluded from the correlation, having inadequate data of monthly BA (less than 5 months on the study period of 2001-2016). However, this type of correlation could have led to clearer results, should the study period have been longer. Also, there could be further development of the fire danger index by accounting for the land use and vegetation type of each gridbox, which could provide more uniformly positive changes in the FWI-BA correlations across the region.

## 7. Conclusions

Summing up, this study focuses on exploring the possibility of an optimized FWI code specifically for the Mediterranean Region, that correlates better with Burned Area and possibly make better fire weather predictions, using future climate projection data.

The results from this study suggest that the correlation between the average monthly FWI values and the monthly logBA values can increase or decrease depending on alterations made on the FWI equations. The alterations of the equations that were experimented with on this study, achieved increased Pearson's  $r$  values of up to 10%.

Since there is not much literature on this topic, this study can pave the way for future research for even more refined optimizations, and could be applied to different regions of the globe.

## 8. References

### Websites

*AFDRS – Australian Fire Danger Rating System.* (n.d.). Retrieved April 12, 2023, from <https://afdrs.com.au>

Canada, N. R. (n.d.). *Canadian wildland fire information system: Canadian forest fire weather index (FWI) system.* Canadian Wildland Fire Information System | Canadian Forest Fire Weather Index (FWI) System. Retrieved March 29, 2023, from <https://cwfis.cfs.nrcan.gc.ca/background/summary/fwi>

Copernicus Climate Change Service, Climate Data Store, (2023): ERA5 hourly data on single levels from 1940 to present. Copernicus Climate Change Service (C3S) Climate Data Store (CDS), Retrieved April 21, 2023 DOI: [10.24381/cds.adbb2d47](https://doi.org/10.24381/cds.adbb2d47)

*Fire weather index (FWI) system.* NWCG. (n.d.). Retrieved April 22, 2023, from <https://www.nwcg.gov/publications/pms437/cffdrs/fire-weather-index-system>

*Land cover.* Land Cover | Copernicus Global Land Service. (2021, September 8). <https://land.copernicus.eu/global/products/lc>

*New dataset ERA5 provides free and detailed information for understanding global climate.* Copernicus. (n.d.). Retrieved April 21, 2023, from <https://climate.copernicus.eu/new-dataset-era5-provides-free-and-detailed-information-understanding-global-climate>

SantanderMetGroup. (n.d.). *Atlas/IPCC-WGI-reference-regions-v4\_coordinates.CSV at main · Santandermetgroup/Atlas.* GitHub. Retrieved April 22, 2023, from [https://github.com/SantanderMetGroup/ATLAS/blob/main/reference-regions/IPCC-WGI-reference-regions-v4\\_coordinates.csv](https://github.com/SantanderMetGroup/ATLAS/blob/main/reference-regions/IPCC-WGI-reference-regions-v4_coordinates.csv)

Schmidt, A. (2021, January 20). *Alps facts.* PBS. <https://www.pbs.org/wnet/nature/blog/alps-facts/>

*The mediterranean marine and coastal environment.* The Mediterranean Marine and Coastal Environment | UNEP MAP QSR. (n.d.). Retrieved March 10, 2023, from <https://www.medqsr.org/mediterranean-marine-and-coastal-environment>

*Welcome to global land cover viewer.* Global Land Cover Viewer. (n.d.). <https://lcviewer.vito.be/2015>

### Journals (Without Link)

Deeming JE, Burgan RE, Cohen JD. 1977. The National Fire-Danger Rating System—1978. USDA Forest Service General technical Report INT-39, Intermountain Forest and Range Experiment Station: Ogden, UT.

Grove, A. T. & O. Rackham, (2001). The nature of Mediterranean Europe: an ecological history. *Journal of Mediterranean Ecology*, 3: 65–68.

Köppen, W. (1936). Das geographische System der Klimate. In: (Köppen, W. & R. Geiger) (Eds). *Handbuch der Klimatologie* 3. (Gebrueder Borntraeger, Berlin, 46 pages).

McArthur, A.G. (1967). Fire Behaviour in Eucalypt Forests. Department of National Development: Forestry and Timber Bureau Leaflet No. 107: Canberra, Australia.

Sneeuwjagt, R.J., Peet, G.B. (1985). Forest Fire Behaviour Tables for Western Australia. Western Australian Department of Conservation and Land Management: Perth, Western Australia.

Turner JA, Lawson BD. (1978). *Weather in the Canadian Forest Fire Danger Rating System*. Environment Canada, Forestry Service: Victoria, British Columbia. Information Report BC-X-177; 37.

Van Wagner, C.E. (1987). Development and structure of the Canadian Forest Fire Weather Index System. Canadian Forestry Service, Headquarters, Ottawa. Forestry Technical Report 35. 35 p.

Van Wagner, C.E., Pickett, T.L. (1985). Equations and FORTRAN program for the Canadian Forest Fire Weather Index System. Canadian Forestry Service, Petawawa National Forestry Institute, Chalk River, Ontario. Forestry Technical Report 33. 18 p.

Van Wagner, C.E. (1972). Equilibrium moisture contents of some fine forest fuels in eastern Canada. Canadian Forestry Service, Petawawa Forest Experiment Station, Chalk River, Ontario. Information Report PS-X-36. 11 p.

Wright, J.M. (1997): Federal meteorological handbook no. 3 (FCM-H3-1997). Office of Federal Coordinator for Meteorological Services and Supporting Research. Washington, DC

### Journals (With Link)

Abatzoglou, J. T., Williams, A. P., Boschetti, L., Zubkova, M., & Kolden, C. A. (2018). Global patterns of interannual climate–fire relationships. *Global Change Biology*, 24(11), 5164–5175. <https://doi.org/10.1111/gcb.14405>

Bedia, J., Golding, N., Casanueva, A., Iturbide, M., Buontempo, C., & Gutiérrez, J. M. (2018). Seasonal predictions of fire weather index: Paving the way for their operational applicability in Mediterranean Europe. *Climate Services*, 9, 101–110. <https://doi.org/10.1016/j.cliser.2017.04.001>

Bonada, N., & Resh, V. H. (2013). Mediterranean-climate streams and rivers: Geographically separated but ecologically comparable freshwater systems. *Hydrobiologia*, 719(1), 1–29. <https://doi.org/10.1007/s10750-013-1634-2>

Chelli, S., Maponi, P., Campetella, G., Monteverde, P., Foglia, M., Paris, E., Lolis, A., & Panagopoulos, T. (2014). Adaptation of the canadian fire weather index to Mediterranean forests. *Natural Hazards*, 75(2), 1795–1810. <https://doi.org/10.1007/s11069-014-1397-8>

Chergui, B., Fahd, S., Santos, X., & Pausas, J. G. (2017). Socioeconomic factors drive fire-regime variability in the Mediterranean Basin. *Ecosystems*, 21(4), 619–628. <https://doi.org/10.1007/s10021-017-0172-6>

DaCamara, C. C., Calado, T. J., Ermida, S. L., Trigo, I. F., Amraoui, M., & Turkman, K. F. (2014). Calibration of the fire weather index over Mediterranean Europe based on fire activity retrieved from MSG satellite imagery. *International Journal of Wildland Fire*, 23(7), 945. <https://doi.org/10.1071/wf13157>

Dimitrakopoulos, A. P., Bemmerzouk, A. M., & Mitsopoulos, I. D. (2011). Evaluation of the canadian fire weather index system in an Eastern Mediterranean environment. *Meteorological Applications*, 18(1), 83–93. <https://doi.org/10.1002/met.214>

Dupuy, J.-luc, Fargeon, H., Martin-StPaul, N., Pimont, F., Ruffault, J., Guijarro, M., Hernando, C., Madrigal, J., & Fernandes, P. (2020). Climate change impact on future wildfire danger and activity in Southern Europe: A Review. *Annals of Forest Science*, 77(2). <https://doi.org/10.1007/s13595-020-00933-5>

Giannaros, T. M., Papavasileiou, G., Lagouvardos, K., Kotroni, V., Dafis, S., Karagiannidis, A., & Dragozi, E. (2022). Meteorological analysis of the 2021 extreme wildfires in Greece: Lessons learned and implications for early warning of the potential for pyroconvection. *Atmosphere*, 13(3), 475. <https://doi.org/10.3390/atmos13030475>

Giglio, L., Boschetti, L., Roy, D. P., Humber, M. L., & Justice, C. O. (2018). The collection 6 modis burned area mapping algorithm and product. *Remote Sensing of Environment*, 217, 72–85. <https://doi.org/10.1016/j.rse.2018.08.005>

Grillakis, M. G. (2019). Increase in severe and extreme soil moisture droughts for Europe under climate change. *Science of The Total Environment*, 660, 1245–1255. <https://doi.org/10.1016/j.scitotenv.2019.01.001>

Grillakis, M., Voulgarakis, A., Rovithakis, A., Seiradakis, K. D., Koutroulis, A., Field, R. D., Kasoar, M., Papadopoulos, A., & Lazaridis, M. (2022). Climate drivers of global wildfire burned area. *Environmental Research Letters*, 17(4), 045021. <https://doi.org/10.1088/1748-9326/ac5fa1>

Hersbach, H., Bell, B., Berrisford, P., Biavati, G., Horányi, A., Muñoz Sabater, J., Nicolas, J., Peubey, C., Radu, R., Rozum, I., Schepers, D., Simmons, A., Soci, C., Dee, D., Thépaut, J.-N. (2023): ERA5 hourly data on single levels from 1940 to present. Copernicus Climate Change Service (C3S) Climate Data Store (CDS), DOI: [10.24381/cds.adbb2d47](https://doi.org/10.24381/cds.adbb2d47) (Accessed on 20-05-2023)

Iturbide, M., Gutiérrez, J. M., Alves, L. M., Bedia, J., Cerezo-Mota, R., Gimeno, E., Cofiño, A. S., Di Luca, A., Faria, S. H., Gorodetskaya, I. V., Hauser, M., Herrera, S., Hennessy, K., Hewitt, H. T., Jones, R. G., Krakovska, S., Manzanar, R., Martínez-Castro, D., Narisma, G. T., ... Vera, C. S. (2020). An update of IPCC climate reference regions for subcontinental analysis of Climate model data: Definition and aggregated datasets. *Earth System Science Data*, 12(4), 2959–2970. <https://doi.org/10.5194/essd-12-2959-2020>

Júnior, J. S. S., Paulo, J. R., Mendes, J., Alves, D., Ribeiro, L. M., & Viegas, C. (2022). Automatic Forest Fire Danger rating calibration: Exploring clustering techniques for regionally customizable fire danger classification. *Expert Systems with Applications*, 193, 116380. <https://doi.org/10.1016/j.eswa.2021.116380>

Karali, A., Hatzaki, M., Giannakopoulos, C., Roussos, A., Xanthopoulos, G., & Tenentes, V. (2014). Sensitivity and evaluation of current fire risk and future projections due to climate change: The case study of Greece. *Natural Hazards and Earth System Sciences*, 14(1), 143–153. <https://doi.org/10.5194/nhess-14-143-2014>

Khlebnikova, E. I. (2009). Objective empiric classifications of earth's climate. *Environmental Structure and Function: Climate System*, 1, 259-270.

Kottek, M., Grieser, J., Beck, C., Rudolf, B., & Rubel, F. (2006). World Map of the Köppen-Geiger climate classification updated. *Meteorologische Zeitschrift*, 15(3), 259–263. <https://doi.org/10.1127/0941-2948/2006/0130>

Lionello, P., Malanotte-Rizzoli, P., Boscolo, R., Alpert, P., Artale, V., Li, L., Luterbacher, J., May, W., Trigo, R., Tsimplis, M., Ulbrich, U., & Xoplaki, E. (2006). The Mediterranean climate: An overview of the main characteristics and issues. *Mediterranean*, 1–26. [https://doi.org/10.1016/s1571-9197\(06\)80003-0](https://doi.org/10.1016/s1571-9197(06)80003-0)

Matthews, S. (2009). A comparison of fire danger rating systems for use in forests. *Australian Meteorological and Oceanographic Journal*, 58(01), 41–48. <https://doi.org/10.22499/2.5801.005>

Michelaki, C., Fyllas, N. M., Galanidis, A., Aloupi, M., Evangelou, E., Arianoutsou, M., & Dimitrakopoulos, P. G. (2020). Adaptive flammability syndromes in Thermo-Mediterranean vegetation,

captured by alternative resource-use strategies. *Science of The Total Environment*, 718, 137437. <https://doi.org/10.1016/j.scitotenv.2020.137437>

Ntinopoulos, N., Spiliotopoulos, M., Vasiliades, L., & Mylopoulos, N. (2022). Contribution to the study of forest fires in semi-arid regions with the use of Canadian fire weather index application in Greece. *Climate*, 10(10), 143. <https://doi.org/10.3390/cli10100143>

Peel, M. C., Finlayson, B. L., & McMahon, T. A. (2007). Updated world map of the Köppen-Geiger climate classification. *Hydrology and Earth System Sciences*, 11(5), 1633–1644. <https://doi.org/10.5194/hess-11-1633-2007>

Peris-Llopis, M., González-Olabarria, J. R., & Mola-Yudego, B. (2020). Size dependency of variables influencing fire occurrence in Mediterranean forests of eastern Spain. *European Journal of Forest Research*, 139(4), 525–537. <https://doi.org/10.1007/s10342-020-01265-9>

Rovithakis, A., Grillakis, M. G., Seiradakis, K. D., Giannakopoulos, C., Karali, A., Field, R., Lazaridis, M., & Voulgarakis, A. (2022). Future climate change impact on wildfire danger over the Mediterranean: The case of Greece. *Environmental Research Letters*, 17(4), 045022. <https://doi.org/10.1088/1748-9326/ac5f94>

Rubel, F., & Kottek, M. (2010). Observed and projected climate shifts 1901-2100 depicted by world maps of the Köppen-Geiger climate classification. *Meteorologische Zeitschrift*, 19(2), 135–141. <https://doi.org/10.1127/0941-2948/2010/0430>

San-Miguel-Ayanz, J., Durrant Houston, T., Boca, R., Liberta`, G., Branco, A., De Rigo, D., Ferrari, D., Maianti, P., Artes Vivancos, T., Costa, H., Lana, F., Loffler, P., Nuijten, D., Leray, T. and Ahlgren, A., Forest Fires in Europe, Middle East and North Africa 2017, EUR 29318 EN, Publications Office of the European Union, Luxembourg, 2018, ISBN 978-92-79-92831-4, doi:10.2760/663443, JRC112831

Wotton, B. M. (2008). Interpreting and using outputs from the Canadian Forest Fire Danger Rating System in Research Applications. *Environmental and Ecological Statistics*, 16(2), 107–131. <https://doi.org/10.1007/s10651-007-0084-2>

Yang, Y., Uddstrom, M., Pearce, G., & Revell, M. (2015). Reformulation of the drought code in the Canadian Fire Weather Index System implemented in New Zealand. *Journal of Applied Meteorology and Climatology*, 54(7), 1523–1537. <https://doi.org/10.1175/jamc-d-14-0090.1>

Zacharakis, I., & Tsihrintzis, V. A. (2023). Environmental forest fire danger rating systems and indices around the globe: A Review. *Land*, 12(1), 194. <https://doi.org/10.3390/land12010194>